Chapter 12
Mass Transport in Porous Media with and Without Chemical Reactions

12.1 Introduction

In this chapter the computation of multispecies (including single-species) mass transport in porous media with chemical reaction in particular is examined. The complexity of those reactive transport processes arising in natural and engineered porous media requires some specific treatment due to their nonlinearity and the occurrence of multiple unknowns. In the preceding Chap. 5 the constitutive relations in form of reversible reaction and irreversible chemical kinetics have been developed. It ends up with a set of mass transport equations for each chemical species $k = 1, \ldots, N$ of an arbitrary number, nonlinearly coupled by the rate expressions of chemical reaction in form of degradation type, Arrhenius type, Monod type or freely editable kinetics. A given species k can be either *mobile* associated with a liquid (aqueous) phase l or *immobile* associated with a solid phase s, so that $N = N^l + N^s$. Chemicals in the liquid phase are subject to advection and dispersion, while in a solid phase there is no advection and dispersion. We solve the reactive multispecies mass transport processes in multi-dimensional porous media under variably saturated, variable-density and nonisothermal conditions. The focus of this chapter is on the treatment of the species mass transport PDE system, while for the flow computations we refer to Chap. 9 for saturated porous media, to Chap. 10 for variably saturated porous media and to Chap. 11 for density-coupled problems. Nonisothermal aspects are subject of Chaps. 11 and 13.

12.2 Basic Equations

12.2.1 3D, Vertical 2D and Axisymmetric Problems

The system of the basic PDE's for 3D and vertical 2D (including axisymmetric) multispecies mass transport in porous media has been developed in Sects. 3.10.5

H.-J.G. Diersch, *FEFLOW*, DOI 10.1007/978-3-642-38739-5_12,

and 5.4 and summarized in Table 3.7. Due to the chemical reaction the equations can be nonlinearly coupled by the kinetic rate laws. The following general system of PDE's results for species $k = 1, \ldots, N^l + N^s$ written for the divergence form of the mass transport equations

$$\begin{aligned} \frac{\partial}{\partial t}(\varepsilon s \Re_k C_k) + \nabla \cdot (\boldsymbol{q} C_k) - \nabla \cdot (\boldsymbol{D}_k \cdot \nabla C_k) + \varepsilon s \vartheta_k \Re_k C_k &= \hat{R}_k + Q_{kw} + Q_k \\ &\quad \text{species } k \text{ of liquid phase } l \\ \frac{\partial}{\partial t}(\varepsilon_s C_k^s) + \varepsilon_s \vartheta_k C_k^s &= \hat{R}_k + Q_k \\ &\quad \text{species } k \text{ of solid phase } s \end{aligned} \tag{12.1}$$

and for the convective form of the mass transport equations

$$\begin{aligned} \varepsilon s \acute{\Re}_k \frac{\partial C_k}{\partial t} + \boldsymbol{q} \cdot \nabla C_k - \nabla \cdot (\boldsymbol{D}_k \cdot \nabla C_k) + (\varepsilon s \vartheta_k \Re_k + Q_h) C_k &= \hat{R}_k + Q_{kw} + Q_k \\ &\quad \text{species } k \text{ of liquid phase } l \\ \varepsilon_s \frac{\partial C_k^s}{\partial t} + \varepsilon_s \vartheta_k C_k^s &= \hat{R}_k + Q_k \\ &\quad \text{species } k \text{ of solid phase } s \end{aligned} \tag{12.2}$$

associated with the constitutive relations[1]

[1] In 3D Cartesian coordinates the components of the mechanical dispersion tensor $\boldsymbol{D}_{\text{mech}}$ for the classic Scheidegger-Bear dispersion model, cf. (3.182), are

$$\begin{aligned} D_{\text{mech},11} &= \tfrac{1}{q}\left(\beta_L q_1^2 + \beta_T q_2^2 + \beta_T q_3^2\right) \\ D_{\text{mech},22} &= \tfrac{1}{q}\left(\beta_T q_1^2 + \beta_L q_2^2 + \beta_T q_3^2\right) \\ D_{\text{mech},33} &= \tfrac{1}{q}\left(\beta_T q_1^2 + \beta_T q_2^2 + \beta_L q_3^2\right) \\ D_{\text{mech},12} &= D_{\text{mech},21} = (\beta_L - \beta_T)\tfrac{q_1 q_2}{q} \\ D_{\text{mech},13} &= D_{\text{mech},31} = (\beta_L - \beta_T)\tfrac{q_1 q_3}{q} \\ D_{\text{mech},23} &= D_{\text{mech},32} = (\beta_L - \beta_T)\tfrac{q_2 q_3}{q} \end{aligned}$$

where $\boldsymbol{q}^T = \left(q_1 \; q_2 \; q_3\right)$ and $q = \|\boldsymbol{q}\|$. In strictly stratified aquifer system, where the transverse dispersion in the vertical x_3-direction can be much smaller than in the horizontal, Burnett and Frind [65] proposed the 3D mechanical dispersion tensor in an alternative form

$$\begin{aligned} D_{\text{mech},11} &= \tfrac{1}{q}\left(\beta_L q_1^2 + \beta_{TH} q_2^2 + \beta_{TV} q_3^2\right) \\ D_{\text{mech},22} &= \tfrac{1}{q}\left(\beta_{TH} q_1^2 + \beta_L q_2^2 + \beta_{TV} q_3^2\right) \\ D_{\text{mech},33} &= \tfrac{1}{q}\left(\beta_{TV} q_1^2 + \beta_{TV} q_2^2 + \beta_L q_3^2\right) \\ D_{\text{mech},12} &= D_{\text{mech},21} = (\beta_L - \beta_{TH})\tfrac{q_1 q_2}{q} \\ D_{\text{mech},13} &= D_{\text{mech},31} = (\beta_L - \beta_{TV})\tfrac{q_1 q_3}{q} \\ D_{\text{mech},23} &= D_{\text{mech},32} = (\beta_L - \beta_{TV})\tfrac{q_2 q_3}{q} \end{aligned}$$

splitting the transverse dispersivity into a horizontal transverse dispersivity β_{TH} and a vertical transverse dispersivity β_{TV}, where it is assumed that $\beta_{TH} \gg \beta_{TV}$. However, as noted by Bear and Cheng [38], Burnett and Find's mechanical dispersion tensor is not consistent with the basic

$$
\begin{aligned}
\boldsymbol{D}_k &= \varepsilon s D_k \boldsymbol{\delta} + \boldsymbol{D}_{\text{mech}} \\
\boldsymbol{D}_{\text{mech}} &= \beta_T \|\boldsymbol{q}\| \boldsymbol{\delta} + (\beta_L - \beta_T) \tfrac{\boldsymbol{q} \otimes \boldsymbol{q}}{\|\boldsymbol{q}\|} \\
\varepsilon_s &= 1 - \varepsilon \\
\Re_k &= 1 + \left(\tfrac{1-\varepsilon}{\varepsilon}\right) \varphi_k \\
\acute{\Re}_k &= 1 + \left(\tfrac{1-\varepsilon}{\varepsilon}\right) \tfrac{\partial(\varphi_k C_k)}{\partial C_k} \\
\varphi_k &= \begin{cases} \kappa_k & \text{Henry} \\ b_k^{\dagger} C_k^{b_k^{\ddagger}-1} & \text{Freundlich} \\ \frac{k_k^{\dagger}}{1+k_k^{\ddagger} C_k} & \text{Langmuir} \end{cases} \quad \text{(Table 3.8)} \\
\hat{R}_k &= \hat{R}_k(\varepsilon, s, C_1^{\alpha}, \ldots, C_N^{\alpha}, T) \quad \alpha \in (l, s)
\end{aligned}
\tag{12.3}
$$

which has to be solved for species concentrations C_k, where for the sake of simplicity we drop the liquid phase index l and the species index k is considered unique in each phase (associated either with liquid l or solid s). In (12.1) and (12.2) a modified bulk reaction rate $\hat{R}_k$ is introduced, in which the linear decay reaction term is separated,[2] $\varepsilon_\alpha \vartheta_k C_k^\alpha$, $\alpha \in (l, s)$, and in addition the (non-reactive, zero-order) well-type SPC term Q_{kw} and a (non-reactive, zero-order) sink/source term are split off, where Q_{kw} is not applied to species of the solid phase. The reaction rate $\hat{R}_k$ is related to the previously defined bulk reaction rate R_k (5.95) and the deduced bulk reaction rate $\tilde{R}_k$ (5.96) via

$$
\begin{aligned}
R_k &= \tilde{R}_k - \textstyle\sum_\alpha \varepsilon_\alpha \vartheta_k C_k^\alpha, \ \alpha \in (l, s) \\
\tilde{R}_k &= \begin{cases} \hat{R}_k + Q_{kw} + Q_k & \text{species } k \text{ of liquid phase } l \\ \hat{R}_k + Q_k & \text{species } k \text{ of solid phase } s \end{cases}
\end{aligned}
\tag{12.4}
$$

Irreversible chemical reaction necessitates specification of rate expression R_k, actually $\hat{R}_k$, where polynomial representations in form of degradation and Arrhenius type kinetics or Monod type kinetics for more complex bio-chemical reaction systems are typical (see Sect. 5.5 for more). For variably saturated porous media additional constitutive relation exists for the saturation $s = s(\psi)$ as a function of pressure head ψ (cf. Sect. 10.2). Notice, in the given formulations of the mass transport equations we preferably use the linear Fick's law of hydrodynamic dispersion, (3.272) with $\Im_H = 0$. Non-Fickian dispersion is commonly related to variable-density problems as discussed in Chap. 11.

We note that usually there is no need to solve mass transport equations for all species N. Only species k of interest will be considered, which are important constituents of the chemical reaction process and/or have impacts on the flow

constitutive relations, such as derived in Sects. 3.8.5.4 and 3.8.5.5, and not conform with tensor transformation rules shown by Lichtner et al. [349].

[2]The separation of the linear decay term allows its numerically implicit treatment in the LHS of the resulting discrete equation system, while nonlinearities appearing in $\hat{R}_k$ require an appropriate iterative approach. Indeed, the reaction rate $\hat{R}_k$ can also incorporate a linear degradation term (in this case ϑ_k should be zero), however, its numerical computation can be less effective than in the direct separation.

and transport regime (e.g., spread and change of contaminants in an environmental flow system). Typically, the transport equations are specified for selected solutes[3](dissolved components) in the liquid phase l and sorbed species at the solid phase s, no more than the essential number of species $N^\star < N$ in total (cf. Sect. 3.9.2). In the above set of mass transport equations for species k occurring either in the liquid phase l or in the solid phase s, it is stipulated that any species k when also subjected to a sorptive equilibrium reaction (retardation) is referred to as a solute constituent in the liquid phase l, while a species exclusively associated with the solid phase s is deemed to be subjected to a (non-equilibrium) reaction kinetics.

The general species mass transport equations (12.1) or (12.2) have to be solved for C_k subject to a set of BC's of Dirichlet, Neumann and Cauchy type as well as well-type SPC (see Sect. 6.3.2), which is for the divergence form

$$\begin{aligned} C_k &= C_{kD} && \text{on} \quad \Gamma_{D_k} \times t[t_0, \infty) \\ (C_k \boldsymbol{q} - \boldsymbol{D}_k \cdot \nabla C_k) \cdot \boldsymbol{n} &= q^\dagger_{kC} && \text{on} \quad \Gamma_{N_k} \times t[t_0, \infty) \\ (C_k \boldsymbol{q} - \boldsymbol{D}_k \cdot \nabla C_k) \cdot \boldsymbol{n} &= -\Phi^\dagger_{kC}(C_{kC} - C_k) && \text{on} \quad \Gamma_{C_k} \times t[t_0, \infty) \\ Q_{kw} &= -\textstyle\sum_w C_{kw} Q_w(t) \delta(\boldsymbol{x} - \boldsymbol{x}_w) && \text{on} \quad \boldsymbol{x}_w \in \Omega \times t[t_0, \infty) \end{aligned} \tag{12.5}$$

and for the convective form

$$\begin{aligned} C_k &= C_{kD} && \text{on} \quad \Gamma_{D_k} \times t[t_0, \infty) \\ -(\boldsymbol{D}_k \cdot \nabla C_k) \cdot \boldsymbol{n} &= q_{kC} && \text{on} \quad \Gamma_{N_k} \times t[t_0, \infty) \\ -(\boldsymbol{D}_k \cdot \nabla C_k) \cdot \boldsymbol{n} &= -\Phi_{kC}(C_{kC} - C_k) && \text{on} \quad \Gamma_{C_k} \times t[t_0, \infty) \\ Q_{kw} &= -\textstyle\sum_w (C_{kw} - C_k) Q_w(t) \delta(\boldsymbol{x} - \boldsymbol{x}_w) && \text{on} \quad \boldsymbol{x}_w \in \Omega \times t[t_0, \infty) \end{aligned} \tag{12.6}$$

where the total boundary is $\Gamma = \Gamma_{C_k} \cup \Gamma_{N_k} \cup \Gamma_{C_k}$, $\forall k$. Note that there are no BC's for the species mass transport equations of the solid phase in (12.1) and

[3]In the special case of a *single-species solute*, where only one dissolved component exists, we can drop the species indicator k and write the governing mass transport equation (12.1) and (12.2), respectively, simply as

$$\begin{aligned} \tfrac{\partial}{\partial t}(\varepsilon s \Re C) + \nabla \cdot (\boldsymbol{q} C) - \nabla \cdot (\boldsymbol{D} \cdot \nabla C) + \varepsilon s \vartheta \Re C &= \hat{R} + Q_{Cw} + Q_C && \text{divergence form} \\ \varepsilon s \acute{\Re} \tfrac{\partial C}{\partial t} + \boldsymbol{q} \cdot \nabla C - \nabla \cdot (\boldsymbol{D} \cdot \nabla C) + (\varepsilon s \vartheta \Re + Q_h) C &= \hat{R} + Q_{Cw} + Q_C && \text{convective form} \end{aligned}$$

with

$$\begin{aligned} \boldsymbol{D} &= \varepsilon s D \boldsymbol{\delta} + \boldsymbol{D}_{\text{mech}} \\ \Re &= 1 + \left(\tfrac{1-\varepsilon}{\varepsilon}\right)\varphi \\ \acute{\Re} &= 1 + \left(\tfrac{1-\varepsilon}{\varepsilon}\right)\tfrac{\partial(\varphi C)}{\partial C} \\ \varphi &= \begin{cases} \kappa & \text{Henry} \\ b^\dagger C^{b^\ddagger - 1} & \text{Freundlich} \\ \frac{k^\dagger}{1 + k^\ddagger C} & \text{Langmuir} \end{cases} \qquad \text{(Table 3.8)} \\ \hat{R} &= \hat{R}(\varepsilon, s, C, T) \end{aligned}$$

for solving the solute concentration C associated with the liquid phase l, where Q_{Cw} and Q_C denote the well-type SPC term and the zero-order mass sink/source term, respectively, for the single-species solute.

(12.2). The normal mass fluxes on Γ_{N_k} and Γ_{C_k} differ between the divergence form and the convective form. As already discussed in Sects. 2.2.2 and 6.3.2 the divergence form imposes the total (advective plus dispersive) boundary mass flux, while the convective form imposes a dispersive mass flux at the boundary. However, the convective form can also be used to express a mass flux BC of an advective load by specifying the Cauchy-type BC in the form

$$-(\boldsymbol{D}_k \cdot \nabla C_k) \cdot \boldsymbol{n} = \underbrace{-\Phi_{kC}}_{\boldsymbol{q}\cdot\boldsymbol{n}} \Big(\underbrace{C_{kC}}_{\frac{q^{\dagger}_{kC}}{\boldsymbol{q}\cdot\boldsymbol{n}}} - C_k \Big) \tag{12.7}$$

to obtain

$$(C_k \boldsymbol{q} - \boldsymbol{D}_k \cdot \nabla C_k) \cdot \boldsymbol{n} = q^{\dagger}_{kC} = (\boldsymbol{q} \cdot \boldsymbol{n}) C_{kC} \tag{12.8}$$

for a given advective normal boundary flux $\boldsymbol{q} \cdot \boldsymbol{n}$ and a boundary concentration C_{kC}, which is equivalent to a Neumann-type BC of the divergence form (cf. Sect. 6.3.2.3). Note further that OBC as discussed in Sect. 6.5.7 represents a special form of Neumann-type BC on $\Gamma_{N_{kO}} \subset \Gamma_{N_k} \subset \Gamma$, which will be treated either as a natural Neumann-type BC with $-(\boldsymbol{D}_k \cdot \nabla C_k) \cdot \boldsymbol{n} \approx 0$ or as implicit OBC (cf. Sect. 8.5.3).

The solution of the governing transient mass transport equations (12.1) and (12.2) requires IC in the form

$$C_k(\boldsymbol{x}, t_0) = C_{k,0}(\boldsymbol{x}) \quad \text{in} \quad \bar{\Omega} \tag{12.9}$$

The essential parameters required for solving (12.1) and (12.2) with (12.5)–(12.9) are listed in Tables I.11 and I.13 of Appendix I. *Steady-state* mass transport conditions occur if $\partial C_k / \partial t$ approaches to zero.[4]

12.2.2 Horizontal 2D Problems

The governing equations for the essentially horizontal, vertically averaged species mass transport in unconfined and confined aquifers have been developed in Sect. 3.10.7 and summarized in Tables 3.10 and 3.11, respectively. The following 2D depth-integrated mass transport equations result

[4]Optionally, FEFLOW suppresses the time derivative term $\partial C_k / \partial t$ for solving steady-state solutions. A specific option exists, named *steady flow – transient transport*, in which the advective flow vector $\boldsymbol{q}$ is invariant with time.

$$\frac{\partial}{\partial t}(\varepsilon\bar{\Re}_k C_k) + \nabla\cdot(\bar{\boldsymbol{q}}C_k) - \nabla\cdot(\bar{\boldsymbol{D}}_k\cdot\nabla C_k) + \varepsilon\vartheta_k\bar{\Re}_k C_k = \bar{\bar{R}}_k + \bar{Q}_{kw} + \bar{Q}_k$$

species k of liquid phase l

$$\frac{\partial}{\partial t}(\varepsilon_s B C_k^s) + \varepsilon_s B\vartheta_k C_k^s = \bar{\hat{R}}_k + \bar{Q}_k$$

species k of solid phase s (12.10)

written in the divergence form and

$$\varepsilon\bar{\Re}_k\frac{\partial C_k}{\partial t} + \bar{\boldsymbol{q}}\cdot\nabla C_k - \nabla\cdot(\bar{\boldsymbol{D}}_k\cdot\nabla C_k) + (\varepsilon\vartheta_k\bar{\Re}_k + \bar{Q}_h)C_k = \bar{\bar{R}}_k + \bar{Q}_{kw} + \bar{Q}_k$$

species k of liquid phase l

$$\varepsilon_s B\frac{\partial C_k^s}{\partial t} + \varepsilon_s B\vartheta_k C_k^s = \bar{\hat{R}}_k + \bar{Q}_k$$

species k of solid phase s (12.11)

written in the convective form, which are associated with the constitutive relations

$$\begin{aligned}
B &= \begin{cases} h - f^B & \text{unconfined} \\ f^T - f^B & \text{confined} \end{cases} \\
\bar{\boldsymbol{D}}_k &= \varepsilon B D_k\boldsymbol{\delta} + \bar{\boldsymbol{D}}_{\text{mech}} \\
\bar{\boldsymbol{D}}_{\text{mech}} &= \beta_T\|\bar{\boldsymbol{q}}\|\boldsymbol{\delta} + (\beta_L - \beta_T)\tfrac{\bar{\boldsymbol{q}}\otimes\bar{\boldsymbol{q}}}{\|\bar{\boldsymbol{q}}\|} \\
\varepsilon_s &= 1 - \varepsilon \\
\bar{\Re}_k &= B\big[1 + \big(\tfrac{1-\varepsilon}{\varepsilon}\big)\varphi_k\big] \\
\bar{\hat{\Re}}_k &= B\big[1 + \big(\tfrac{1-\varepsilon}{\varepsilon}\big)\tfrac{\partial(\varphi_k C_k)}{\partial C_k}\big] \\
\varphi_k &= \begin{cases} \kappa_k & \text{Henry} \\ b_k^\dagger C_k^{b_k^\ddagger - 1} & \text{Freundlich} \\ \frac{k_k^\dagger}{1 + k_k^\ddagger C_k} & \text{Langmuir} \end{cases} \quad \text{(Table 3.8)} \\
\bar{\bar{R}}_k &= B\hat{R}_k \\
\hat{R}_k &= \hat{R}_k(\varepsilon, s, C_1^\alpha, \ldots, C_N^\alpha, T) \quad \alpha \in (l, s)
\end{aligned} \tag{12.12}$$

where similarly the deduced bulk reaction rate $\bar{\bar{R}}_k = \bar{\hat{R}}_k + \bar{Q}_{kw} + \bar{Q}_k$ is suitably split into a depth-integrated bulk reaction rate $\bar{\hat{R}}_k$, a depth-integrated well-type SPC term $\bar{Q}_{kw}$ and a depth-integrated zero-order sink/source term for species k, where $\bar{Q}_{kw}$ is not applied to species in the solid phase. The solution of (12.10) or (12.11) for the species concentration C_k is associated with the following BC's of Dirichlet, Neumann and Cauchy type as well as well-type SPC

$$\begin{aligned}
C_k &= C_{kD} && \text{on} \quad \Gamma_{D_k}\times t[t_0,\infty) \\
(C_k\bar{\boldsymbol{q}} - \bar{\boldsymbol{D}}_k\cdot\nabla C_k)\cdot\boldsymbol{n} &= \bar{q}_{kC}^\dagger && \text{on} \quad \Gamma_{N_k}\times t[t_0,\infty) \\
(C_k\bar{\boldsymbol{q}} - \bar{\boldsymbol{D}}_k\cdot\nabla C_k)\cdot\boldsymbol{n} &= -\bar{\Phi}_{kC}^\dagger(C_{kC} - C_k) && \text{on} \quad \Gamma_{C_k}\times t[t_0,\infty) \\
\bar{Q}_{kw} &= -\textstyle\sum_w C_{kw}Q_w(t)\delta(\boldsymbol{x} - \boldsymbol{x}_w) && \text{on} \quad \boldsymbol{x}_w\in\Omega\times t[t_0,\infty)
\end{aligned} \tag{12.13}$$

written for the divergence form of the mass transport equation and

$$\begin{aligned} C_k &= C_{kD} && \text{on} \quad \Gamma_{D_k} \times t[t_0, \infty) \\ -(\bar{\boldsymbol{D}}_k \cdot \nabla C_k) \cdot \boldsymbol{n} &= \bar{q}_{kC} && \text{on} \quad \Gamma_{N_k} \times t[t_0, \infty) \\ -(\bar{\boldsymbol{D}}_k \cdot \nabla C_k) \cdot \boldsymbol{n} &= -\bar{\Phi}_{kC}(C_{kC} - C_k) && \text{on} \quad \Gamma_{C_k} \times t[t_0, \infty) \\ \bar{Q}_{kw} &= -\textstyle\sum_w (C_{kw} - C_k) Q_w(t) \delta(\boldsymbol{x} - \boldsymbol{x}_w) && \text{on} \quad \boldsymbol{x}_w \in \Omega \times t[t_0, \infty) \end{aligned} \tag{12.14}$$

written for the convective form of the mass transport equation, imposed on $\Gamma = \Gamma_{C_k} \cup \Gamma_{N_k} \cup \Gamma_{C_k}$, $\forall k$, and with the IC of the form

$$C_k(\boldsymbol{x}, t_0) = C_{k,0}(\boldsymbol{x}) \quad \text{in} \quad \bar{\Omega} \tag{12.15}$$

The essential parameters required for solving (12.10) and (12.11) with (12.13), (12.14) and (12.15) are listed in Tables I.12 and I.14 of Appendix I.

12.3 Finite Element Formulation

In Chap. 8 the fundamental concepts of FEM are exemplified for an ADE of a scalar quantity, which is paradigmatic for the present species mass transport equations. Based on these principles given there we use now the GFEM to solve the governing mass transport equations (12.1) and (12.2) associated with the corresponding BC's (12.5), (12.6) and IC's (12.9). Since most of the details are equivalent to the ADE developments given in Chap. 8 we shall focus here only on aspects featuring the reactive multispecies mass transport. For convenience we restrict our developments to 3D, vertical 2D and axisymmetric mass transport problems (Sect. 12.2.1). The formulations for the horizontal 2D mass transport in unconfined and confined aquifers (Sect. 12.2.2) will appear rather similar and can be easily deduced from the given statements.

12.3.1 Weak Forms

According to Sect. 8.5 we can find analogously to the statements (8.48) and (8.55) the corresponding weak forms for the governing multispecies mass transport equation written in the divergence form (12.1) as

$$\int_\Omega w \frac{\partial(\varepsilon s \Re_k C_k)}{\partial t} d\Omega - \int_\Omega C_k \boldsymbol{q} \cdot \nabla w d\Omega + \int_\Omega \nabla w \cdot (\boldsymbol{D}_k \cdot \nabla C_k) d\Omega +$$

$$\int_\Omega w(\varepsilon s \vartheta_k \Re_k C_k - \hat{R}_k - Q_k) d\Omega + \sum_w w(\boldsymbol{x}_w) Q_w(t) C_{kw} +$$

$$\int_{\Gamma_{N_k}} w q^{\dagger}_{kC} d\Gamma - \int_{\Gamma_{C_k}} w \Phi^{\dagger}_{kC} (C_{kC} - C_k) d\Gamma = 0, \quad \forall w \in H^1_0(\Omega) \tag{12.16}$$

$$\int_{\Omega} w \frac{\partial (\varepsilon_s C^s_k)}{\partial t} d\Omega + \int_{\Omega} w (\varepsilon_s \vartheta_k C^s_k - \hat{R}_k - Q_k) d\Omega = 0, \quad \forall w \in H^1_0(\Omega) \tag{12.17}$$

and written in the convective form (12.2) as

$$\int_{\Omega} w \varepsilon s \acute{\Re}_k \frac{\partial C_k}{\partial t} d\Omega + \int_{\Omega} w \boldsymbol{q} \cdot \nabla C_k d\Omega + \int_{\Omega} \nabla w \cdot (\boldsymbol{D}_k \cdot \nabla C_k) d\Omega +$$

$$\int_{\Omega} w [(\varepsilon s \vartheta_k \Re_k + Q_h) C_k - \hat{R}_k - Q_k] d\Omega + \sum_w w(\boldsymbol{x}_w) Q_w(t) (C_{kw} - C_k) +$$

$$\int_{\Gamma_{N_k}} w q_{kC} d\Gamma - \int_{\Gamma_{C_k}} w \Phi_{kC} (C_{kC} - C_k) d\Gamma = 0, \quad \forall w \in H^1_0(\Omega) \tag{12.18}$$

$$\int_{\Omega} w \varepsilon_s \frac{\partial C_k}{\partial t} d\Omega + \int_{\Omega} w (\varepsilon_s \vartheta_k C^s_k - \hat{R}_k - Q_k) d\Omega = 0, \quad \forall w \in H^1_0(\Omega) \tag{12.19}$$

where w is a suitable weighting function and the boundary integrals are suitably separated into their segments $\Gamma = \Gamma_{D_k} \cup \Gamma_{N_k} \cup \Gamma_{C_k}$ imposed by the Dirichlet, Neumann and Cauchy-type BC's (12.5) and (12.6). OBC on $\Gamma_{N_{kO}} \subset \Gamma_{N_k}$ represents special implementations of Neumann-type BC.[5]

[5] A boundary with OBC on $\Gamma_{N_{kO}}$ can be separated from the Neumann boundary Γ_{N_k} so that for the divergence form

$$\int_{\Gamma_{N_k}} w q^{\dagger}_{kC} d\Gamma = \int_{\Gamma_{N_k} \setminus \Gamma_{N_{kO}}} w q^{\dagger}_{kC} d\Gamma + \int_{\Gamma_{N_{kO}}} w (C_k \boldsymbol{q} - \boldsymbol{D}_k \cdot \nabla C_k) \cdot \boldsymbol{n} d\Gamma$$

and for the convective form

$$\int_{\Gamma_{N_k}} w q_{kC} d\Gamma = \int_{\Gamma_{N_k} \setminus \Gamma_{N_{kO}}} w q_{kC} d\Gamma - \int_{\Gamma_{N_{kO}}} w (\boldsymbol{D}_k \cdot \nabla C_k) \cdot \boldsymbol{n} d\Gamma$$

The implicit treatment of OBC requires the incorporation of the $\Gamma_{N_{kO}}$−integrals into the LHS of the resulting matrix system (see below). In contrast, a natural Neumann-type BC with $-(\boldsymbol{D}_k \cdot \nabla C_k) \cdot \boldsymbol{n} \approx 0$ on $\Gamma_{N_{kO}}$ is often the preferred alternative formulation for an OBC. Note, however, that for both cases in the divergence form the boundary flux $\boldsymbol{q} \cdot \boldsymbol{n}$ must be known a priori. The boundary flux $\boldsymbol{q} \cdot \boldsymbol{n}$ can be either explicitly given from a Neumann-type BC $q_h = \boldsymbol{q} \cdot \boldsymbol{n}$ for flow or must be computed by a postprocessing budget evaluation of the flow equation on the corresponding outflowing boundary section imposed by Dirichlet-type or Cauchy-type BC of flow.

12.3.2 GFEM and Resulting Nonlinear Matrix System

The weak statements (12.3.1)–(12.19) involve the unknown variable C_k of each species k occurring either on the liquid phase l or solid phase s. In using the FEM this variable is replaced by a *continuous approximation* that assumes the separability of space and time (see Sect. 8.4). Thus

$$C_k(\boldsymbol{x},t) \approx \sum_j N_j(\boldsymbol{x}) C_{kj}(t), \quad j = 1,\ldots,N_\mathrm{P},\ k = 1,\ldots,N \tag{12.20}$$

where j designates global nodal indices. Using the Galerkin method with the weighting function

$$w \to w_i = N_i, \quad i = 1,\ldots,N_\mathrm{P} \tag{12.21}$$

and applying the approximate solutions (12.20) in (12.3.1)–(12.19), we obtain the following matrix systems of each N_P equations (cf. Sect. 8.9) for each species k as follows

$$\boldsymbol{H}_k(\boldsymbol{C})\cdot\dot{\boldsymbol{C}}_k + \boldsymbol{E}_k(\boldsymbol{C})\cdot\boldsymbol{C}_k - \boldsymbol{R}_k(\boldsymbol{C}) = \boldsymbol{0} \quad (k = 1,\ldots,N) \tag{12.22}$$

or

$$\begin{aligned}
\boldsymbol{H}_1(\boldsymbol{C}_1,\ldots,\boldsymbol{C}_N)\cdot\dot{\boldsymbol{C}}_1 + \boldsymbol{E}_1(\boldsymbol{C}_1,\ldots,\boldsymbol{C}_N)\cdot\boldsymbol{C}_1 - \boldsymbol{R}_1(\boldsymbol{C}_1,\ldots,\boldsymbol{C}_N) &= \boldsymbol{0}\\
\boldsymbol{H}_2(\boldsymbol{C}_1,\ldots,\boldsymbol{C}_N)\cdot\dot{\boldsymbol{C}}_2 + \boldsymbol{E}_2(\boldsymbol{C}_1,\ldots,\boldsymbol{C}_N)\cdot\boldsymbol{C}_2 - \boldsymbol{R}_2(\boldsymbol{C}_1,\ldots,\boldsymbol{C}_N) &= \boldsymbol{0}\\
\boldsymbol{H}_3(\boldsymbol{C}_1,\ldots,\boldsymbol{C}_N)\cdot\dot{\boldsymbol{C}}_3 + \boldsymbol{E}_3(\boldsymbol{C}_1,\ldots,\boldsymbol{C}_N)\cdot\boldsymbol{C}_3 - \boldsymbol{R}_3(\boldsymbol{C}_1,\ldots,\boldsymbol{C}_N) &= \boldsymbol{0}\\
&\vdots\\
\boldsymbol{H}_N(\boldsymbol{C}_1,\ldots,\boldsymbol{C}_N)\cdot\dot{\boldsymbol{C}}_N + \boldsymbol{E}_N(\boldsymbol{C}_1,\ldots,\boldsymbol{C}_N)\cdot\boldsymbol{C}_N - \boldsymbol{R}_N(\boldsymbol{C}_1,\ldots,\boldsymbol{C}_N) &= \boldsymbol{0}
\end{aligned} \tag{12.23}$$

and alternatively written in a compact form as

$$\boldsymbol{H}(\boldsymbol{C})\cdot\dot{\boldsymbol{C}} + \boldsymbol{E}(\boldsymbol{C})\cdot\boldsymbol{C} - \boldsymbol{R}(\boldsymbol{C}) = \boldsymbol{0} \tag{12.24}$$

or

$$\begin{pmatrix} \boldsymbol{H}_1 & \boldsymbol{0} & \boldsymbol{0} & \ldots & \boldsymbol{0} \\ \boldsymbol{0} & \boldsymbol{H}_2 & \boldsymbol{0} & \ldots & \boldsymbol{0} \\ \boldsymbol{0} & \boldsymbol{0} & \boldsymbol{H}_3 & \ldots & \boldsymbol{0} \\ & & & \ddots & \\ \boldsymbol{0} & \boldsymbol{0} & \boldsymbol{0} & \ldots & \boldsymbol{H}_N \end{pmatrix} \cdot \begin{pmatrix} \dot{\boldsymbol{C}}_1 \\ \dot{\boldsymbol{C}}_2 \\ \dot{\boldsymbol{C}}_3 \\ \vdots \\ \dot{\boldsymbol{C}}_N \end{pmatrix} + \begin{pmatrix} \boldsymbol{E}_1 & \boldsymbol{0} & \boldsymbol{0} & \ldots & \boldsymbol{0} \\ \boldsymbol{0} & \boldsymbol{E}_2 & \boldsymbol{0} & \ldots & \boldsymbol{0} \\ \boldsymbol{0} & \boldsymbol{0} & \boldsymbol{E}_3 & \ldots & \boldsymbol{0} \\ & & & \ddots & \\ \boldsymbol{0} & \boldsymbol{0} & \boldsymbol{0} & \ldots & \boldsymbol{E}_N \end{pmatrix} \cdot \begin{pmatrix} \boldsymbol{C}_1 \\ \boldsymbol{C}_2 \\ \boldsymbol{C}_3 \\ \vdots \\ \boldsymbol{C}_N \end{pmatrix} - \begin{pmatrix} \boldsymbol{R}_1 \\ \boldsymbol{R}_2 \\ \boldsymbol{R}_3 \\ \vdots \\ \boldsymbol{R}_N \end{pmatrix} = \begin{pmatrix} \boldsymbol{0} \\ \boldsymbol{0} \\ \boldsymbol{0} \\ \vdots \\ \boldsymbol{0} \end{pmatrix} \tag{12.25}$$

with

$$\boldsymbol{C}_k = \begin{pmatrix} C_{k1} \\ C_{k2} \\ \vdots \\ C_{kN_\mathrm{P}} \end{pmatrix}, \quad \dot{\boldsymbol{C}}_k = \begin{pmatrix} \frac{dC_{k1}}{dt} \\ \frac{dC_{k2}}{dt} \\ \vdots \\ \frac{dC_{kN_\mathrm{P}}}{dt} \end{pmatrix}, \quad \boldsymbol{C} = \begin{pmatrix} \boldsymbol{C}_1 \\ \boldsymbol{C}_2 \\ \boldsymbol{C}_3 \\ \vdots \\ \boldsymbol{C}_N \end{pmatrix}, \quad \dot{\boldsymbol{C}} = \begin{pmatrix} \dot{\boldsymbol{C}}_1 \\ \dot{\boldsymbol{C}}_2 \\ \dot{\boldsymbol{C}}_3 \\ \vdots \\ \dot{\boldsymbol{C}}_N \end{pmatrix} \tag{12.26}$$

showing the major nonlinearities in parentheses, where the matrices and RHS vectors are given for species k of the liquid phase l as

$$\begin{aligned}
\boldsymbol{H}_k &= H_{ij,k} = \begin{cases} \sum_e \int_{\Omega^e} \varepsilon^e s^e \Re_k^e(C^e)\, N_i N_j \, d\Omega^e & \text{divergence form} \\ \sum_e \int_{\Omega^e} \varepsilon^e s^e \acute{\Re}_k^e(C^e)\, N_i N_j \, d\Omega^e & \text{convective form} \end{cases} \\
\boldsymbol{E}_k &= E_{ij,k} = \begin{cases} \sum_e \Big(-\int_{\Omega^e} \boldsymbol{q}^e \cdot \nabla N_i N_j \, d\Omega^e + \int_{\Omega^e} \nabla N_i \cdot (\boldsymbol{D}_k^e \cdot \nabla N_j) d\Omega^e + \\ \quad \int_{\Omega^e} \big[\varepsilon^e s^e \vartheta_k^e \Re_k^e(C^e) + \frac{\partial (\varepsilon^e s^e \Re_k^e(C^e))}{\partial t} \big] N_i N_j \, d\Omega^e + \\ \quad \int_{\Gamma^e_{C_k}} \Phi^{\dagger e}_{kC} N_i N_j \, d\Gamma^e + \int_{\Gamma^e_{N_{kO}}} N_i (\boldsymbol{q}^e N_j - \boldsymbol{D}_k^e \cdot \nabla N_j) \cdot \boldsymbol{n} d\Gamma^e \Big) & \text{divergence form} \\ \sum_e \Big(\int_{\Omega^e} N_i \boldsymbol{q}^e \cdot \nabla N_j \, d\Omega^e + \int_{\Omega^e} \nabla N_i \cdot (\boldsymbol{D}_k^e \cdot \nabla N_j) d\Omega^e + \\ \quad \int_{\Omega^e} [\varepsilon^e s^e \vartheta_k^e \Re_k^e(C^e) + Q_h^e] N_i N_j \, d\Omega^e + \\ \quad \int_{\Gamma^e_{C_k}} \Phi^e_{kC} N_i N_j \, d\Gamma^e - \int_{\Gamma^e_{N_{kO}}} N_i (\boldsymbol{D}_k^e \cdot \nabla N_j) \cdot \boldsymbol{n} d\Gamma^e \Big) - \delta_{ij} Q_w(t)\big|_i & \text{convective form} \end{cases} \\
\boldsymbol{R}_k &= R_{i,k} = \begin{cases} \sum_e \Big(\int_{\Omega^e} N_i [\hat{R}_k^e(C^e) + Q_k^e] d\Omega^e + \int_{\Gamma^e_{C_k}} N_i \Phi^{\dagger e}_{kC} C^e_{kC} d\Gamma^e - \\ \quad \int_{\Gamma^e_{N_k} \setminus \Gamma^e_{N_{kO}}} N_i q^{\dagger e}_{kC} d\Gamma^e \Big) - C_{kw} Q_w(t)\big|_i & \text{divergence form} \\ \sum_e \Big(\int_{\Omega^e} N_i [\hat{R}_k^e(C^e) + Q_k^e] d\Omega^e + \int_{\Gamma^e_{C_k}} N_i \Phi^e_{kC} C^e_{kC} d\Gamma^e - \\ \quad \int_{\Gamma^e_{N_k} \setminus \Gamma^e_{N_{kO}}} N_i q^e_{kC} d\Gamma^e \Big) - C_{kw} Q_w(t)\big|_i & \text{convective form} \end{cases}
\end{aligned} \tag{12.27}$$

and for species k of the solid phase s as

$$\begin{aligned}
\boldsymbol{H}_k &= H_{ij,k} = \sum_e \int_{\Omega^e} \varepsilon_s^e \, N_i N_j \, d\Omega^e \\
\boldsymbol{E}_k &= E_{ij,k} = \begin{cases} \sum_e \int_{\Omega^e} \big(\varepsilon_s^e \vartheta_k^e + \frac{\partial \varepsilon_s^e}{\partial t} \big) N_i N_j \, d\Omega^e & \text{divergence form} \\ \sum_e \int_{\Omega^e} \varepsilon_s^e \vartheta_k^e N_i N_j \, d\Omega^e & \text{convective form} \end{cases} \\
\boldsymbol{R}_k &= R_{i,k} = \sum_e \int_{\Omega^e} N_i [\hat{R}_k^e(C^e) + Q_k^e] d\Omega^e
\end{aligned} \tag{12.28}$$

in which $(i, j = 1, \ldots, N_P)$ and $(e = 1, \ldots, N_E)$, $\boldsymbol{H}_k = \boldsymbol{H}_k(\boldsymbol{C})$ $(k = 1, \ldots, N)$ are the nonlinear symmetric storage matrices including retardation effects for species k occurring in the liquid phase l, $\boldsymbol{E}_k = \boldsymbol{E}_k(\boldsymbol{C})$ $(k = 1, \ldots, N)$ are the unsymmetric 'conductance' matrices encompassing advection, dispersion and retardation effects for species k occurring in the liquid phase l as well as linear decay for species k in both the liquid phase l and the solid phase s, and $\boldsymbol{R}_k = \boldsymbol{R}_k(\boldsymbol{C})$ $(k = 1, \ldots, N)$ are the chemical rate vectors, which represent nonlinear dependencies on the total concentration vector $\boldsymbol{C}$ according to the considered reaction kinetics. We note that there is no advection and dispersion for species k belonging to the solid phase s. The integrals appearing in (12.27) and (12.28) are integrated on element level in the local coordinates as described in Sect. 8.12. Analytical evaluations of partial integral terms of (12.27) and (12.28) can be deduced from developments done in Appendix H for selected element types. The differential elements $d\Omega^e$ and $d\Gamma^e$ differ for 3D, 2D and axisymmetric problems as given by (8.122)–(8.124), respectively. Is is important to note that the resulting global system of equations (12.24) is *unsymmetric* since the matrix $\boldsymbol{E}$ is unsymmetric due to advection.

The matrix system (12.24) can be highly nonlinear mainly due to the dependence of the reaction rate vector $\boldsymbol{R}$ on $\boldsymbol{C}$ so that an efficient numerical solution strategy is required, in particular for reactive multispecies transport problems.[6] One possibility would be the solution of the coupled matrix system (12.24) in a direct and simultaneous manner. Although mathematically rigorous, practical implementation of that approach is limited and not generally applicable to large, geometrically complex and multidimensional problems because of the significant memory and/or computational burden. The size of the coefficient matrices $\boldsymbol{H}$ and $\boldsymbol{E}$ in the discretized system (12.24) grows as a product of the number of nodes N_P and the number of applied species N. In general, the direct approach involves solving a $N_P \times N$ system of nonlinear equations at each time plane. Furthermore, the system for a simultaneous solution can be ill-conditioned due to the significantly different scales of the processes involved. Alternatively, in order to reduce the computational requirements, a *decoupled* (or split-operator) solution strategy is preferred, in which the species equations are solved sequentially by using efficient iteration techniques. Kanney et al. [299] discussed different strategies of such split-operator approaches. Among a variety of split-operator techniques the sequential iterative approach (SIA) have proven superior and powerful. In FEFLOW, we prefer an adaptive error-controlled SIA strategy which is based on an efficient predictor-corrector time-stepping technique. In contrast to a common SIA technique the transport equations with the reaction terms are solved in an adaptive full time interval using predictor solutions to linearize the nonlinear reaction terms. The overall iteration control is

[6] For single-species solute transport (12.24) and (12.22) reduce to simplified matrix system, where nonlinearities can only occur due to nonlinear retardation (Freundlich or Langmuir adsorption isotherms) and/or higher-order kinetic reactions, however, subjected to the same species of solute.

fully embedded in a time-marching strategy via a sophisticated error-based time-step adaptation.

For advective-dominant mass transport the discretized system (12.24) can be easily combined with upwind strategies as introduced in Sect. 8.14. Useful upwind strategies refer to the SU and FU methods (Sect. 8.14.3), SC method (Sect. 8.14.4) and PGLS method (Sect. 8.14.5), in which the tensor of mechanical dispersion $\boldsymbol{D}_{\text{mech}}$ as part of the hydrodynamic dispersion tensor $\boldsymbol{D}_k$ is appropriately modified by stabilization terms in dependence on the actual spatial and temporal discretizations or concentration gradients. The required modifications of $\boldsymbol{D}^e_{\text{mech}}$ for each element e were discussed in the preceding Sect. 11.6.3 and summarized in Table 11.3.

12.3.3 *Adaptive SIA-Based Solution Strategy for Multispecies Mass Transport Embedded in the GLS Predictor-Corrector Time Integrator*

The GLS predictor-corrector time integrator (Sect. 8.13.4) with automatically adapted time stepping has been shown very cost-efficient and robust for classes of nonlinear systems such as variably saturated problems (Sect. 10.7.5) and/or variable-density flow (Sect. 11.6.4). We also prefer this technique[7] for solving the present transient chemically reactive systems. At a multispecies presence ($N^\star > 1$)

[7] Alternatively to the GLS predictor-corrector method, the time integration of (12.22) for each species k by using the simple $\theta-$method (Sect. 8.13.4) gives

$$\begin{aligned}&\left(\tfrac{\boldsymbol{H}_k(\boldsymbol{C}_{n+1})}{\Delta t_n} + \boldsymbol{E}_k(\boldsymbol{C}_{n+1})\theta\right)\cdot \boldsymbol{C}_{k,n+1} = \\ &\left(\tfrac{\boldsymbol{H}_k(\boldsymbol{C}_{n+1})}{\Delta t_n} - \boldsymbol{E}_k(\boldsymbol{C}_{n+1})(1-\theta)\right)\cdot \boldsymbol{C}_{k,n} + \left(\boldsymbol{R}_k(\boldsymbol{C}_{n+1})\theta + \boldsymbol{R}_k(\boldsymbol{C}_n)(1-\theta)\right)\end{aligned}$$

where $\theta \in (\frac{1}{2}, 1)$ for the Crank-Nicolson and the fully implicit scheme, respectively. For chemically reactive processes a nonlinear matrix system $\boldsymbol{R}^\star_{k,n+1} = \boldsymbol{A}_k(\boldsymbol{C}_{n+1})\cdot \boldsymbol{C}_{k,n+1} - \boldsymbol{Z}_k(\boldsymbol{C}_{n+1}, \boldsymbol{C}_n) = \boldsymbol{0}$ results, which must be iteratively solved either via the Picard method (Sect. 8.18.1)

$$\boldsymbol{A}_k(\boldsymbol{C}^\tau_{n+1})\cdot \boldsymbol{C}^{\tau+1}_{k,n+1} = \boldsymbol{Z}_k(\boldsymbol{C}^\tau_{n+1}, \boldsymbol{C}_n) \quad \tau = 0, 1, 2, \ldots$$

or via the Newton method (Sect. 8.18.2)

$$\begin{aligned}\boldsymbol{J}_k(\boldsymbol{C}^\tau_{n+1})\cdot \Delta\boldsymbol{C}^\tau_{k,n+1} &= -\boldsymbol{R}^\star_{k,n+1}(\boldsymbol{C}^\tau_{n+1}, \boldsymbol{C}_n) \quad \tau = 0, 1, 2, \ldots \\ \Delta\boldsymbol{C}^\tau_{k,n+1} &= \boldsymbol{C}^{\tau+1}_{k,n+1} - \boldsymbol{C}^\tau_{k,n+1} \\ \boldsymbol{J}_k(\boldsymbol{C}^\tau_{n+1}) &= \tfrac{\partial \boldsymbol{R}^\star_{k,n+1}(\boldsymbol{C}^\tau_{n+1}, \boldsymbol{C}_n)}{\partial \boldsymbol{C}^\tau_{k,n+1}}\end{aligned}$$

until satisfactory convergence is achieved for the iterations τ at each given time stage $n+1$. Note that this iterative solution strategy is also applicable to *steady-state* mass transport problems if setting $\theta = 1$ and $\Delta t_n \to \infty$.

the solution is performed in a decoupled manner, where each $k-$species nonlinear matrix system (12.22) is sequentially solved and appropriately linearized by using the adaptive predictor-corrector time-stepping strategy consisting of the following working steps:

STEP 0: Initialization

Computation of the initial acceleration vectors $\dot{\boldsymbol{C}}_{k,0}$ for time plane $n = 0$ (once per $k-$species equation)

$$\boldsymbol{H}_k(\boldsymbol{C}_0) \cdot \dot{\boldsymbol{C}}_{k,0} = -\boldsymbol{E}_k(\boldsymbol{C}_0) \cdot \boldsymbol{C}_{k,0} + \boldsymbol{R}_k(\boldsymbol{C}_0) \quad (k = 1, \ldots, N) \tag{12.29}$$

and guessing an initial time step Δt_0. The initial systems (12.29) are solved with the initial concentration vector $\boldsymbol{C}_0^T = (\boldsymbol{C}_{1,0}\ \boldsymbol{C}_{2,0}\ \boldsymbol{C}_{3,0}\ \ldots\ \boldsymbol{C}_{N,0})$ known by the IC's (12.9) for each species k. They need to be solved only once at initial time t_0.

STEP 1: Predictor solutions

Perform explicit predictor solutions for all species k by using the 1st-order accurate FE and 2nd-order accurate AB scheme, respectively,

$$\boldsymbol{C}_{k,n+1}^{p} = \begin{cases} \boldsymbol{C}_{k,n} + \Delta t_n \dot{\boldsymbol{C}}_{k,n} & \text{FE predictor} \\ \boldsymbol{C}_{k,n} + \frac{\Delta t_n}{2}\left[\left(2 + \frac{\Delta t_n}{\Delta t_{n-1}}\right)\dot{\boldsymbol{C}}_{k,n} - \frac{\Delta t_n}{\Delta t_{n-1}}\dot{\boldsymbol{C}}_{k,n-1}\right] & \text{AB predictor} \end{cases} \tag{12.30}$$

where the superposed p denotes the predictor values at the new time plane $n+1$. Note that, since $\dot{\boldsymbol{C}}_{k,n-1}$ is required, the AB formula cannot be applied before the second step ($n = 1$). The prediction has to be started with the FE scheme, where $\dot{\boldsymbol{C}}_{k,0}$ is available from (12.29).

STEP 2: Corrector solutions

Do corrector solutions for the nonlinear matrix system (12.22) of each species k via the TR or BE scheme by applying the predictor solution $\boldsymbol{C}_{n+1}^{p\,T} = (\boldsymbol{C}_{1,n+1}^{p\,T}, \boldsymbol{C}_{2,n+1}^{p\,T}, \boldsymbol{C}_{3,n+1}^{p\,T}, \ldots, \boldsymbol{C}_{N,n+1}^{p\,T})$ from (12.30) to linearize the species equations as

$$\left(\frac{\boldsymbol{H}_k(\boldsymbol{C}_{n+1}^{p})}{\theta \Delta t_n} + \boldsymbol{E}_k(\boldsymbol{C}_{n+1}^{p})\right) \cdot \boldsymbol{C}_{k,n+1} =$$

$$\boldsymbol{H}_k(\boldsymbol{C}_{n+1}^{p}) \cdot \left[\frac{\boldsymbol{C}_{k,n}}{\theta \Delta t_n} + \left(\tfrac{1}{\theta} - 1\right)\dot{\boldsymbol{C}}_{k,n}\right] + \boldsymbol{R}_k(\boldsymbol{C}_{n+1}^{p}) \tag{12.31}$$

to determine the concentration $\boldsymbol{C}_{k,n+1}$ for each species k at the new time plane $n+1$, where $\theta \in (\frac{1}{2}, 1)$ for the TR and BE scheme, respectively.

STEP 3: Updated accelerations

Update the new acceleration vectors for each species k by inverting the FE and BE, respectively:

$$\dot{\boldsymbol{C}}_{k,n+1} = \begin{cases} \frac{\boldsymbol{C}_{k,n+1}-\boldsymbol{C}_{k,n}}{\Delta t_n} & \text{FE} \\ \left(2-\frac{\Delta t_{n-1}}{\Delta t_n+\Delta t_{n-1}}\right)\left(\frac{\boldsymbol{C}_{k,n+1}-\boldsymbol{C}_{k,n}}{\Delta t_n}\right)-\left(\frac{\Delta t_n}{\Delta t_n+\Delta t_{n-1}}\right)\left(\frac{\boldsymbol{C}_{k,n}-\boldsymbol{C}_{k,n-1}}{\Delta t_{n-1}}\right) & \text{AB} \end{cases} \tag{12.32}$$

to obtain $\dot{\boldsymbol{C}}_{k,n+1}$ at the new time plane $n+1$.

STEP 4: Error estimation

Compute the LTE for the FE/BE and AB/TR scheme as a function of the corrector and predictor solutions for each species k in the form (cf. Table 8.7)

$$\boldsymbol{d}_{k,n+1} = \varphi(\boldsymbol{C}_{k,n+1} - \boldsymbol{C}^{p}_{k,n+1}) \tag{12.33}$$

with

$$\varphi = \begin{cases} \frac{1}{2} & \text{for FE/BE} \\ \frac{1}{3\left(1+\frac{\Delta t_{n-1}}{\Delta t_n}\right)} & \text{for AB/TR} \end{cases} \tag{12.34}$$

Suitable error norms are applied to the LTE vector $\boldsymbol{d}_{k,n+1}$ for each species k. Commonly, the weighted RMS L_2 error norm

$$\|\boldsymbol{d}_{k,n+1}\|_{L_2} = \left[\frac{1}{N_{\mathrm{P}}}\left(\sum_{i=1}^{N_{\mathrm{P}}}\left|\frac{d_{k,i,n+1}}{C_{k,\max,n+1}}\right|^2\right)\right]^{1/2} \tag{12.35}$$

and the maximum L_∞ error norm

$$\|\boldsymbol{d}_{k,n+1}\|_{L_\infty} = \frac{1}{C_{k,\max,n+1}} \max_i |d_{k,i,n+1}| \tag{12.36}$$

are chosen, where $C_{k,\max,n+1}$ corresponds to the maximum values of $k-$species concentration detected at the time plane $n+1$ and used to normalize the solution vector.

STEP 5: Tactic of time stepping and error control

Predict the potential new $k-$specific time-step lengths by means of the error estimate (12.33) for each species k, the current time step size Δt_n and a user-specified error tolerance ϵ as:

$$\Delta t_{k,n+1} = \Delta t_n \left(\frac{\epsilon}{\|\boldsymbol{d}_{k,n+1}\|_{L_p}}\right)^{1/\lambda} \tag{12.37}$$

where

$$\lambda = \begin{cases} 2 & \text{for FE/BE} \\ 3 & \text{for AB/TR} \end{cases} \qquad p = \begin{cases} 2 & \text{for RMS error norm} \\ \infty & \text{for maximum error norm} \end{cases} \tag{12.38}$$

The following criteria are used to monitor the progress of the nonlinear solution:

(1) If

$$\Delta t_{k,n+1} \geq \Delta t_n \tag{12.39}$$

the solution $\boldsymbol{C}_{k,n+1}$ for the species equation k is accurate within the error bound defined by ϵ and the increase of the time step is always accepted.

(2) Else if

$$\gamma \Delta t_n \leq \Delta t_{k,n+1} < \Delta t_n \tag{12.40}$$

where γ is typically 0.85, the kth solution $\boldsymbol{C}_{k,n+1}$ is accepted but the time step is not changed, i.e., $\Delta t_{k,n+1} = \Delta t_n$.

(3) Else if

$$\Delta t_{k,n+1} < \gamma \Delta t_n \tag{12.41}$$

the solution $\boldsymbol{C}_{k,n+1}$ cannot be accepted within the required error tolerance ϵ and has to be rejected. The proposed new time step size (12.37) has to be reduced according to

$$\Delta t^{\text{red}}_{k,n+1} = \frac{\Delta t_n^2}{\Delta t_{n+1}} \left(\frac{\epsilon}{\|\boldsymbol{d}_{k,n+1}\|_{L_p}} \right)^{\varsigma} \quad (\varsigma = 1 \text{ for FE/BE and } \varsigma = 2/3 \text{ for AB/TR}) \tag{12.42}$$

and the solution of all species k must be repeated for the time plane $n + 1$ with $\Delta t_n = \min_k (\Delta t^{\text{red}}_{k,n+1})$.

(4) If the criteria (12.39) and (12.40) are satisfied by all species equations and the solutions $\boldsymbol{C}_{k,n+1}$ can be accepted for all species k within the required error tolerance ϵ, the new time step is determined from the minimum of the $k-$specific time step lengths, viz.,

$$\Delta t_{n+1} = \min_k (\Delta t_{k,n+1}) \tag{12.43}$$

and the time stepping procedure proceeds to the new time plane $n + 2$ with the time step Δt_{n+1} (12.43).

It is important to note that the error tolerance ϵ is the only user-specified parameter to control the entire nonlinear and transient solution process. The starting-up phase is still influenced by the initial time step Δt_0 which should be kept small. In practice, two further constraints for the time-step size have shown to be useful. Firstly, the time step should not exceed a maximum measure, i.e., $\Delta t_{n+1} \leq \Delta t_{\max}$. Secondly, the rate for changing the time-step size $\Xi = \Delta t_{n+1}/\Delta t_n$ can also be limited, where $\Xi > 1$ can be 2, 3 or even more. Using these constraints the actually increased new time step results as $\Delta t_{n+1}^{\text{actual}} = \min(\Delta t_{n+1}, \Delta t_{\max}, \Xi \Delta t_n)$.

The predictor-corrector strategy fully monitors the nonlinear and transient solution process via the time LTE in which the size of the time step is cheaply and automatically varied in accordance with the overall accuracy requirements. The time step is increased whenever possible and decreased only when necessary. It is evident to note that by monitoring the temporal accuracy requirements, at the same time the solution strategy provides an efficient control of the nonlinearities of the species transport equation system via the predictor solutions. Due to the power of the predictor-corrector strategy any additional iterative feedback within the adapted time steps can be avoided.

12.4 Mass Budget Analysis

We use the CBFM, as introduced in Sect. 8.19.2, for obtaining a precise mass budget analysis. It is based on the specific weak formulations of the governing mass transport equations. The corresponding boundary mass fluxes on Γ have to be evaluated from the basic weak statements (12.3.1) and (12.18) of the divergence and convective form, respectively, written as

$$\int_\Gamma N_i \, q^\dagger_{n_{kC}} \, d\Gamma = -\int_\Omega N_i \frac{\partial(\varepsilon s \Re_k C_k)}{\partial t} d\Omega + \int_\Omega C_k \boldsymbol{q} \cdot \nabla N_i \, d\Omega - \int_\Omega \nabla N_i \cdot (\boldsymbol{D}_k \cdot \nabla C_k) d\Omega - \int_\Omega N_i (\varepsilon s \vartheta_k \Re_k C_k - \hat{R}_k - Q_k) d\Omega - C_{kw} Q_w(t)|_i \qquad (12.44)$$

$$\int_\Gamma N_i \, q_{n_{kC}} \, d\Gamma = -\int_\Omega N_i \varepsilon s \acute{\Re}_k \frac{\partial C_k}{\partial t} d\Omega - \int_\Omega N_i \boldsymbol{q} \cdot \nabla C_k \, d\Omega - \int_\Omega \nabla N_i \cdot (\boldsymbol{D}_k \cdot \nabla C_k) d\Omega - \int_\Omega N_i [(\varepsilon s \vartheta_k \Re_k + Q_h) C_k - \hat{R}_k - Q_k] d\Omega - (C_{kw} - C_k) Q_w(t)|_i \qquad (12.45)$$

to compute $q^\dagger_{n_{kC}}$ or $q_{n_{kC}}$, where C_k is known at evaluation time t_{n+1}. Note that the boundary mass flux $q^\dagger_{n_{kC}} = (C_k \boldsymbol{q} - \boldsymbol{D}_k \cdot \nabla C_k) \cdot \boldsymbol{n}$ of the divergence form

encompasses the total mass flux consisting of the advective and dispersive parts, while the boundary mass flux $q_{n_kC} = -(\boldsymbol{D}_k \cdot \nabla C_k) \cdot \boldsymbol{n}$ of the convective form consists only of the dispersive part. Thus, for the convective form we need an additional balance expression of the missing advective part $q^a_{n_kC} = C_k \boldsymbol{q} \cdot \boldsymbol{n}$ to obtain $q^\dagger_{n_kC} = q_{n_kC} + q^a_{n_kC}$. This is attained by using an auxiliary weak formulation applied to the governing flow equation (10.5) as described in Sect. 8.19.2.4. It yields

$$\begin{aligned}\int_\Gamma N_i\, q^a_{n_kC}\, d\Gamma = &-\int_\Omega \nabla N_i \cdot [k_r \boldsymbol{K} f_\mu \cdot (\nabla h + \chi \boldsymbol{e})] C_k\, d\Omega - \\ &\int_\Omega N_i \nabla C_k \cdot [k_r \boldsymbol{K} f_\mu \cdot (\nabla h + \chi \boldsymbol{e})] d\Omega + \\ \int_\Omega N_i C_k (Q_h + Q_{hw} + Q_{\mathrm{EOB}}) d\Omega &- \int_\Omega N_i C_k \Big(s S_o \frac{\partial h}{\partial t} + \varepsilon \frac{\partial s}{\partial t} \Big) d\Omega \end{aligned} \tag{12.46}$$

to compute $q^a_{n_kC}$, where h, s and C_k are known at evaluation time t_{n+1}. Expanding the boundary flux on Γ as described in Sect. 8.19.2 the following matrix system results to solve the consistent boundary total mass flux vector $\boldsymbol{q}^\dagger_{n_kC}$ for each species k, viz.,

$$\begin{aligned}\boldsymbol{M} \cdot \boldsymbol{q}^\dagger_{n_kC} = &-\boldsymbol{H}_k(\boldsymbol{C}) \cdot \dot{\boldsymbol{C}}_k - \boldsymbol{E}^\dagger_k(\boldsymbol{C}) \cdot \boldsymbol{C}_k + \boldsymbol{R}^\dagger_k(\boldsymbol{C}) \\ &- \begin{cases} \boldsymbol{0} & \text{divergence form} \\ \boldsymbol{V}(\boldsymbol{h}) \cdot \boldsymbol{C}_k + \boldsymbol{A}(\boldsymbol{C}_k) \cdot \boldsymbol{h} - \boldsymbol{F}(\boldsymbol{C}_k, \boldsymbol{s}, \dot{\boldsymbol{h}}, \dot{\boldsymbol{s}}) & \text{convective form} \end{cases} \end{aligned} \tag{12.47}$$

for known $\boldsymbol{C}_k$, $\dot{\boldsymbol{C}}_k$, $\boldsymbol{h}$, $\dot{\boldsymbol{h}}$, $\boldsymbol{s}$ and $\dot{\boldsymbol{s}}$ at the corresponding evaluation time t_{n+1}, where $\boldsymbol{H}_k$ is defined in (12.27) and

$$\begin{aligned}\boldsymbol{M} = M_{ij} &= \textstyle\int_\Gamma N_i N_j\, d\Gamma \\ \boldsymbol{E}^\dagger_k = E^\dagger_{ij,k} &= \begin{cases} -\int_\Omega \boldsymbol{q} \cdot \nabla N_i N_j\, d\Omega + \int_\Omega \nabla N_i \cdot (\boldsymbol{D}_k \cdot \nabla N_j) d\Omega + \\ \int_\Omega (\varepsilon s \vartheta_k \Re_k + \frac{\partial(\varepsilon s \Re_k)}{\partial t}) N_i N_j\, d\Omega & \text{divergence form} \\ \int_\Omega N_i \boldsymbol{q} \cdot \nabla N_j\, d\Omega + \int_\Omega \nabla N_i \cdot (\boldsymbol{D}_k \cdot \nabla N_j) d\Omega + \\ \int_\Omega (\varepsilon s \vartheta_k \Re_k + Q_h) N_i N_j\, d\Omega - \delta_{ij} Q_w(t)\big|_i & \text{convective form} \end{cases} \\ \boldsymbol{R}^\dagger_k = R^\dagger_{i,k} &= \textstyle\int_\Omega N_i (\hat{R}_k + Q_k) d\Omega - C_{kw} Q_w(t)\big|_i \\ \boldsymbol{V} = V_{ij} &= \textstyle\int_\Omega N_i \nabla N_j \cdot [k_r \boldsymbol{K} f_\mu \cdot (\nabla h + \chi \boldsymbol{e})] d\Omega \\ \boldsymbol{A} = A_{ij} &= \textstyle\int_\Omega \nabla N_i \cdot [k_r \boldsymbol{K} f_\mu \cdot (\nabla N_j + \chi \boldsymbol{e})] C_k\, d\Omega \\ \boldsymbol{F} = F_i &= \textstyle\int_\Omega N_i C_k \big(Q_h + Q_{\mathrm{EOB}} - s S_o \frac{\partial h}{\partial t} - \varepsilon \frac{\partial s}{\partial t} \big) d\Omega - C_k Q_w(t)\big|_i \end{aligned} \tag{12.48}$$

in which ($i, j = 1, \ldots, N_{\mathrm{P}}$), ($e = 1, \ldots, N_{\mathrm{E}}$) and ($k = 1, \ldots, N$). Note that $\boldsymbol{V}$, $\boldsymbol{A}$ and $\boldsymbol{F}$ are only needed for the convective form. In the budget analysis the integral

boundary balance flux $\boldsymbol{Q}_{n_{kC}}$ is directly evaluated at each boundary node by

$$\begin{aligned}\boldsymbol{Q}_{n_{kC}} &= -\boldsymbol{M}\cdot\boldsymbol{q}^{\dagger}_{n_{kC}}\\ &= \boldsymbol{H}_k(\boldsymbol{C})\cdot\dot{\boldsymbol{C}}_k + \boldsymbol{E}^{\dagger}_k(\boldsymbol{C})\cdot\boldsymbol{C}_k - \boldsymbol{R}^{\dagger}_k(\boldsymbol{C})\\ &\quad + \begin{cases}\boldsymbol{0} & \text{divergence form}\\ \boldsymbol{V}(\boldsymbol{h})\cdot\boldsymbol{C}_k + \boldsymbol{A}(\boldsymbol{C}_k)\cdot\boldsymbol{h} - \boldsymbol{F}(\boldsymbol{C}_k,\boldsymbol{s},\dot{\boldsymbol{h}},\dot{\boldsymbol{s}}) & \text{convective form}\end{cases}\end{aligned} \tag{12.49}$$

where $\boldsymbol{Q}_{n_{kC}}$ corresponds to the nodal vector of the integral boundary mass flux.

12.5 Examples

12.5.1 Single-Species Solute Advective-Dispersive-Decay Transport in a Column

Considering a 1D column of homogeneous saturated porous medium in which a single-species solute intrudes with a constant concentration C_D, the flow in the column is maintained at a constant flux $q = \varepsilon v$ and in addition, the solute in the column continuously undergoes linear decay ϑ and linear adsorption $\Re$, then the governing mass transport equation (12.2) written in 1D $x-$coordinate reduces to

$$\Re\frac{\partial C}{\partial t} + v\frac{\partial C}{\partial x} - \mathcal{D}\frac{\partial^2 C}{\partial x^2} - \Re\vartheta C = 0 \tag{12.50}$$

with $v = \frac{q}{\varepsilon}$, $\mathcal{D} = D + \beta_L v$ and $\Re = 1 + (\frac{1-\varepsilon}{\varepsilon})\kappa$, for which the following analytical solution exists [33, 396, 540][8]

[8] Since the complementary error function erfc() is often in combination with exp(), it is numerically useful to introduce the function exf(a,b) defined as

$$\text{exf}(a,b) = \exp(a)\text{erfc}(b)$$

which is suitably approximated as follows [540]:

$$\text{exf}(a,b) \approx \begin{cases}\exp(a-b^2)(a_1\tau + a_2\tau^2 + a_3\tau^3 + a_4\tau^4 + a_5\tau^5) & \text{if } 0 \le b \le 3\\ \frac{1}{\sqrt{\pi}}\exp(a-b^2)/(b + 0.5/(b + 1/(b + 1.5/(b + 2/(b + 2.5/(b + 1)))))) & \text{if } b > 3\\ 2\exp(a) - \text{exf}(a,-b) & \text{if } b < 0\\ 0 \quad \text{if } |a| > 170 \text{ and } b \le 0 \text{ or } |a-b^2| > 170 \text{ and } b > 0 & \end{cases}$$

where $\tau = 1/(1 + 0.3275911b)$ and $a_1 = 0.2548296$, $a_2 = -0.2844967$, $a_3 = 1.421414$, $a_4 = -1.453152$ and $a_5 = 1.061405$.

Table 12.1 Parameters and conditions used for the single-species solute advective-dispersive-decay transport in a column

Quantity	Symbol	Value	Unit
Column length	L	100	m
Constant flux	q	0.1	$\mathrm{m\,d^{-1}}$
Porosity	ε	0.2	1
Constant velocity	$v = \frac{q}{\varepsilon}$	0.5	$\mathrm{m\,d^{-1}}$
Henry sorption coefficient	κ	0.1	1
Retardation	$\Re = 1 + (\frac{1-\varepsilon}{\varepsilon})\kappa$	1.4	1
Decay rate	ϑ	$2 \cdot 10^{-8}$	$\mathrm{s^{-1}}$
Molecular diffusion	D	0	$\mathrm{m^2\,s^{-1}}$
Longitudinal dispersivity	β_L	0.1	m
Dispersion	$\mathcal{D} = D + \beta_L v$	$5.787 \cdot 10^{-7}$	$\mathrm{m^2\,s^{-1}}$
IC and BC's			
Initial condition (IC) of C	C_0	0	$\mathrm{mg\,l^{-1}}$
Dirichlet-type BC at $x = 0$	C_D	1	$\mathrm{mg\,l^{-1}}$
Natural BC at $x = L$	$q_{n_C} = -\mathcal{D}\nabla C \cdot \boldsymbol{n}$	0	$\mathrm{gm^{-2}\,d^{-1}}$
FEM			
Space increment	Δx	0.1	m
Initial time step size	Δt_0	10^{-4}	d
RMS error tolerance (AB/TR and FE/BE)	ϵ	10^{-4}	1
Simulation time period	t_{end}	200	d

$$C(x,t) = \tfrac{1}{2}C_D\left[\exp\left(\frac{(v-u)x}{2\mathcal{D}}\right)\operatorname{erfc}\left(\frac{\Re x - ut}{2\sqrt{\mathcal{D}\Re t}}\right) + \exp\left(\frac{(v+u)x}{2\mathcal{D}}\right)\operatorname{erfc}\left(\frac{\Re x + ut}{2\sqrt{\mathcal{D}\Re t}}\right)\right] \tag{12.51}$$

with

$$u = v\sqrt{1 + \frac{4\vartheta\Re\mathcal{D}}{v^2}}, \quad \operatorname{erfc}(a) = \tfrac{2}{\sqrt{\pi}}\int_a^\infty \exp(-\xi^2)d\xi \tag{12.52}$$

associated with the IC and BC's

$$C(x,0) = 0, \quad C(0,t) = C_D, \quad \tfrac{\partial C}{\partial x}(\infty,t) = 0 \tag{12.53}$$

to solve $C(x,t)$.

The analytical solution (12.51) will be compared with numerical results by using the parameters as summarized in Table 12.1. For the numerical simulations a uniform spatial discretization consisting of linear elements is used. The mesh is chosen sufficiently dense so that no upwinding is required. The adaptive GLS predictor-corrector time integrator is preferred, where both the 2nd-order accurate AB/TR and the 1st-order accurate FE/BE scheme are tested.

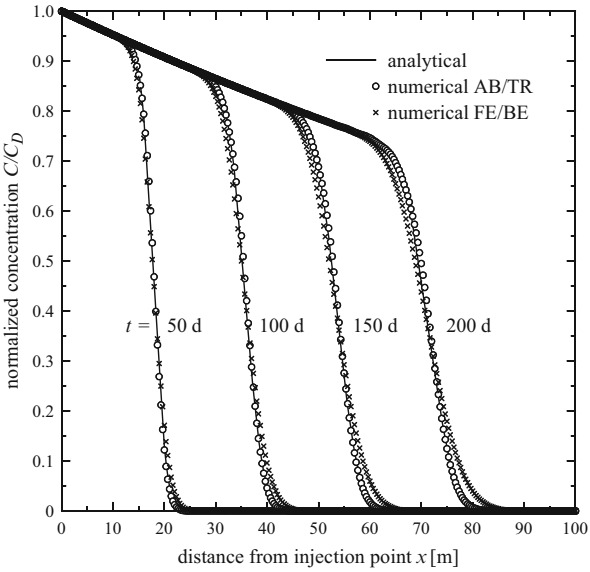

Fig. 12.1 Simulated versus analytical concentration profiles at different times t in days (single-species solute advective-dispersive-decay transport)

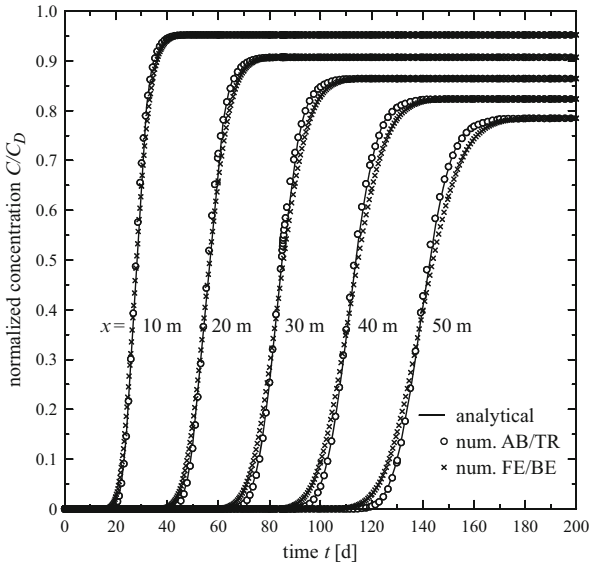

Fig. 12.2 Simulated versus analytical breakthrough curves at different distances x from injection point in meters (single-species solute advective-dispersive-decay transport)

The achieved numerical results in comparison with the analytical solutions are shown in Figs. 12.1 and 12.2. The agreements are rather well, in particular for the AB/TR scheme. Differences for the lower accurate FE/BE time stepping are revealed at later times, which indicate temporal discretization effects by numerical dispersion in the order $\mathcal{O}(\frac{\Delta t_n}{2} v^2)$ (cf. Sect. 8.15). The simulations over the period of

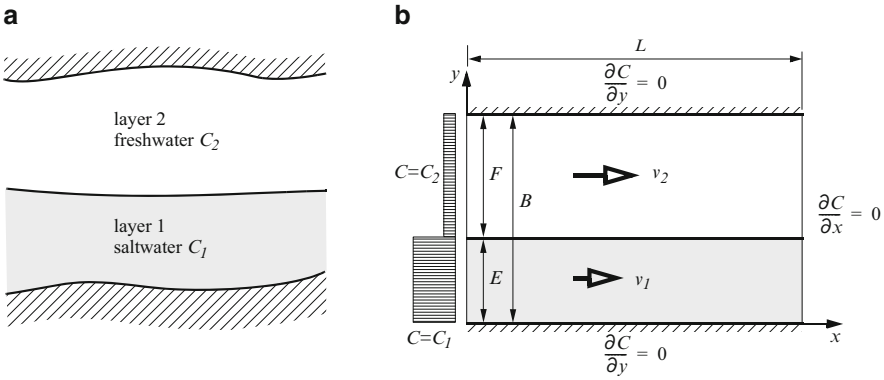

Fig. 12.3 Paradigmatic bilayered aquifer structure: (**a**) principal undisturbed state and (**b**) schematic sketch (Modified from [513])

200 days required 210 time steps for the AB/TR scheme and 502 time steps for the FE/BE scheme.

12.5.2 Hydrodispersive Mixing of Single-Species Solute in a Bilayered Aquifer

Thiele and Diersch [513] studied a principal paradigmatic problem as illustrated in Fig. 12.3 for a confined alluvial aquifer having a bilayered structure, where the upper layer contains groundwater with lower salinity (freshwater) while in the underlying layer saline groundwater (saltwater) occurs. The major objective is to analyze the mechanism of transverse mixing the freshwater and saltwater flow under uniform (and possibly different) velocities in the two layers. Analytical solutions given by Thiele and Diersch [513] can be used to verify computational results when neglecting density effects and excluding chemical reaction.

For the present problem the governing mass transport equation (12.2) written in 2D $x-y-$coordinates reduces to

$$\Re \frac{\partial C}{\partial t} + v_x \frac{\partial C}{\partial x} - \mathcal{D}_{xx} \frac{\partial^2 C}{\partial x^2} - \mathcal{D}_{yy} \frac{\partial^2 C}{\partial y^2} = 0 \tag{12.54}$$

with $v_x = \frac{q_x}{\varepsilon}$, $\mathcal{D}_{xx} = D + \beta_L v_x$ and $\mathcal{D}_{yy} = D + \beta_T v_x$, where $C = C(x, y, t)$ represents the concentration of the single-species solute (salinity) to be solved. Note that $\mathcal{D}_{xy} = \mathcal{D}_{yx} = 0$ since $v_y = 0$ assuming an ideally $x-$parallel flow in the aquifer layers. Imposing the following IC and BC's

inhomogeneous IC:

$$C(x,y,0) = \begin{cases} C_1 & (0 \le y \le E) \\ C_2 & (E < y \le B) \end{cases}, \quad (0 \le x \le L) \tag{12.55}$$

BC's:

$$C(0,y,t) = \begin{cases} C_1 & (0 \le y \le E) \\ C_2 & (E < y \le B) \end{cases} \tag{12.56}$$

$$\frac{\partial}{\partial x}C(L,y,t) = 0,\ \frac{\partial}{\partial y}C(x,0,t) = 0,\ \frac{\partial}{\partial y}C(x,B,t) = 0\ \ (0 \le x \le L,\ 0 \le y \le B) \tag{12.57}$$

an analytical solution for the case of uniform velocity $v = v_x = v_1 = v_2$ and neglected molecular diffusion $D = 0$ can be derived [513]:

$$\frac{C(x,y,t) - C_2}{C_1 - C_2} = \frac{E}{B} + \sum_{i=1}^{\infty}\Bigg\{\frac{1}{i\pi}\sin\Big(i\pi\frac{E}{B}\Big)\cos\Big(i\pi\frac{y}{B}\Big)\Big[\exp\Big(\frac{x}{2\beta_L}(1-I_i)\Big)\operatorname{erfc}\Big(\frac{x - I_i vt}{2\sqrt{v\beta_L t}}\Big) + \exp\Big(\frac{x}{2\beta_L}(1+I_i)\Big)\operatorname{erfc}\Big(\frac{x + I_i vt}{2\sqrt{v\beta_L t}}\Big)\Big] + \frac{2}{i\pi}\sin\Big(i\pi\frac{E}{B}\Big)\cos\Big(i\pi\frac{y}{B}\Big)\exp\Big(-i^2\pi^2\frac{v\beta_T t}{B^2}\Big) \times \Big[1 - \tfrac{1}{2}\operatorname{erfc}\Big(\frac{x - I_i vt}{2\sqrt{v\beta_L t}}\Big) - \tfrac{1}{2}\exp\Big(\frac{x}{\beta_L}\Big)\operatorname{erfc}\Big(\frac{x + I_i vt}{2\sqrt{v\beta_L t}}\Big)\Big]\Bigg\} \tag{12.58}$$

with

$$I_i = \sqrt{1 + \frac{4i^2\pi^2}{B^2}\beta_L\beta_T} \tag{12.59}$$

In using a homogeneous IC in form of $C(x,y,0) = C_2\ (0 \le x \le L,\ 0 \le y \le B)$ different to (12.55), (12.58) reduces to the Bruch and Street's analytical solution [60]

$$\frac{C(x,y,t) - C_2}{C_1 - C_2} = \frac{E}{2B}\Big[\operatorname{erfc}\Big(\frac{x - vt}{2\sqrt{v\beta_L t}}\Big) + \exp\Big(\frac{x}{\beta_L}\Big)\operatorname{erfc}\Big(\frac{x + vt}{2\sqrt{v\beta_L t}}\Big)\Big] + \sum_{i=1}^{\infty}\Bigg\{\frac{1}{i\pi}\sin\Big(i\pi\frac{E}{B}\Big)\cos\Big(i\pi\frac{y}{B}\Big)\Big[\exp\Big(\frac{x}{2\beta_L}(1-I_i)\Big)\operatorname{erfc}\Big(\frac{x - I_i vt}{2\sqrt{v\beta_L t}}\Big) + \exp\Big(\frac{x}{2\beta_L}(1+I_i)\Big)\operatorname{erfc}\Big(\frac{x + I_i vt}{2\sqrt{v\beta_L t}}\Big)\Big]\Bigg\} \tag{12.60}$$

More complex analytical solution is given by Thiele and Diersch [513] for nonuniform $x-$parallel velocities $v_1 \neq v_2$ occurring in the two layers. Note that for evaluating the analytical exp(.)erfc(.) expressions appearing in (12.58) and (12.60) the more suitable exf(.,.) function is used as already introduced in Sect. 12.5.1.

Table 12.2 Parameters and conditions used for the bilayered aquifer problem

Quantity	Symbol	Value	Unit
Domain shown in Fig. 12.3 with settings			
Domain length	L	3,500	m
Aquifer thickness	B	30	m
Layer 1 thickness	E	10	m
Layer 2 thickness	F	20	m
Constant horizontal flux	$q = q_x$	0.15	$\mathrm{m\,d^{-1}}$
Porosity	ε	0.3	1
Constant horizontal velocity	$v = \frac{q}{\varepsilon}$	0.5	$\mathrm{m\,d^{-1}}$
Retardation	$\Re$	1	1
Decay rate	ϑ	0	$\mathrm{s^{-1}}$
Molecular diffusion	D	0	$\mathrm{m^2\,s^{-1}}$
Longitudinal dispersivity	β_L	5	m
Transverse dispersivity	β_T	0.5	m
IC and BC			
Initial condition (IC) of C (12.55)	$C_0 = \begin{cases} C_1 & (0 \le y \le E) \\ C_2 & (E < y \le B) \end{cases}$	$\begin{cases} 1 \\ 0 \end{cases}$	$\mathrm{mg\,l^{-1}}$
Dirichlet-type BC at $x = 0$ (12.56)	$C_D = \begin{cases} C_1 & (0 \le y \le E) \\ C_2 & (E < y \le B) \end{cases}$	$\begin{cases} 1 \\ 0 \end{cases}$	$\mathrm{mg\,l^{-1}}$
FEM			
Nonuniform 2D mesh of $1{,}000 \times 70$ linear and quadratic quadrilateral elements, GFEM			
Initial time step size	Δt_0	10^{-4}	d
RMS error tolerance (AB/TR)	ϵ	10^{-4}	1
Simulation time period	t_{end}	2,400	d

To compare the numerical results to the analytical solution (12.59) we simulate the mixing process in the bilayered aquifer for the case of a constant uniform (steady-state) velocity $v = v_x = v_1 = v_2$ with parameters and conditions as listed in Table 12.2. Unspecified BC's represent boundaries, at which natural BC's are imposed (12.57). The 2D cross-sectional model domain is appropriately discretized by $1{,}000 \times 70$ quadrilateral elements of both linear and quadratic element type. The structured mesh is uniformly discretized in $x-$direction $\Delta x = L/1{,}000$, however, in $y-$direction at the layer contact the element thickness Δy is about 4 cm and gradually increases with the distance from the interface. The computations are performed with GFEM without any upwind and the adaptive GLS AB/TR predictor-corrector time stepping. For the matrix equation solution the direct Gaussian elimination method is preferred.

The simulated breakthrough behavior in comparison to the analytical solution (12.58) is shown in Fig. 12.4 for two different points located in the upper layer 2. It reveals a typical nonmonothonic 'overshooting' characteristic resulting from the inhomogeneous IC (12.55) in which the lower layer 1 is fully pre-salinated at initial time. Those overshooting effects are thoroughly studied by Thiele and Diersch [513], even for nonuniform velocities in the aquifer layers. As shown in Fig. 12.4 the agreement with the analytical solution is rather well both for linear elements and

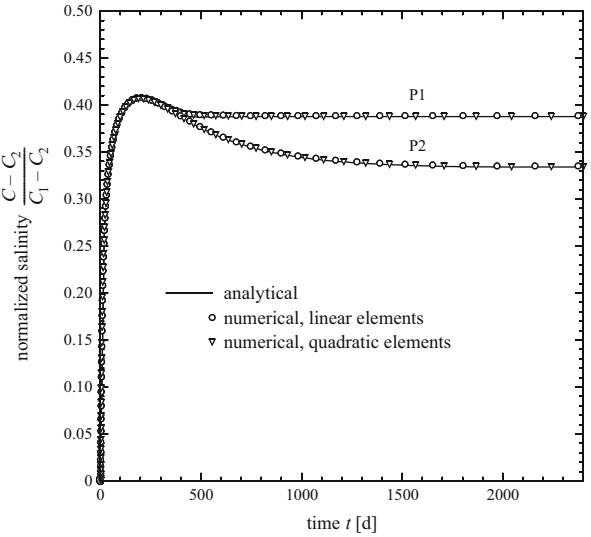

Fig. 12.4 Simulated versus analytical breakthrough curves of salinity $\frac{C-C_2}{C_1-C_2}$ at two different points P1$(x, y) = (200\,\text{m}, 12\,\text{m})$ and P2$(x, y) = (1{,}000\,\text{m}, 12\,\text{m})$ in a bilayered confined aquifer with uniform velocity $v = v_1 = v_2$ and inhomogeneous IC (12.55)

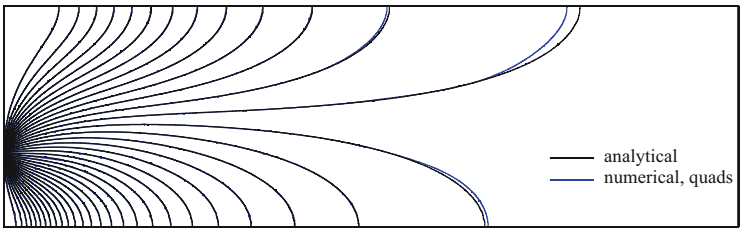

Fig. 12.5 Simulated salinity contours $\frac{C-C_2}{C_1-C_2}$ at $t = 2{,}400$ d in comparison to the analytical distribution (vertical exaggeration 10:1, shown domain ranges $0 \le x \le 1{,}000\,\text{m}$, $0 \le y \le B = 30\,\text{m}$) using inhomogeneous IC (12.55). Simulation results based on quadratic element mesh. Used contouring interval of normalized salinity is 0.025

somewhat better for quadratic elements. This is also illustrated in Fig. 12.5 for the simulated salinity contours in comparison to the analytical distribution. It indicates the fully mixing of salinity in the two layers for large distances x and elapsed times t approaching to a value of $(E\,C_1 + F\,C_2)/B = 0.3333$.

To expose the breakthrough behavior in contrast to the pre-salinated state of layer 1, Fig. 12.6 exhibits the salinity history at two points in layer 2 for the case in which both layers are filled by freshwater from beginning. Now, it reveals a monothonic increase of salinity without any overshoots. The attained numerical findings are shown in good agreement with the analytical solution, which is in this case given by Bruch and Street's expression (12.60).

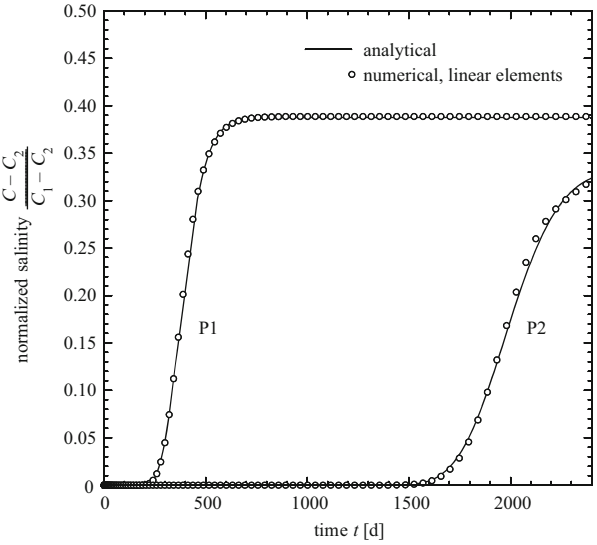

Fig. 12.6 Simulated versus analytical breakthrough curves of salinity $\frac{C-C_2}{C_1-C_2}$ at two different points P1$(x, y) = (200\,\text{m}, 12\,\text{m})$ and P2$(x, y) = (1{,}000\,\text{m}, 12\,\text{m})$ in a bilayered confined aquifer with uniform velocity $v = v_1 = v_2$ and homogeneous IC: $C_0 = C_2 = 0$

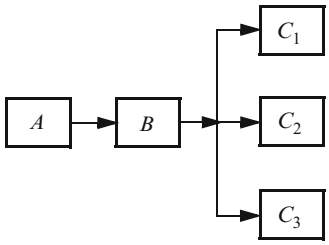

Fig. 12.7 Serial-parallel reaction network by Sun et al. [504]

12.5.3 Multispecies Mass Transport with Comparison to Analytical Solutions

12.5.3.1 Sun et al.'s 1D Serial-Parallel Reaction Problem

Sun et al. [504] present analytical solutions for 1D multispecies transport problems with serial and parallel reaction kinetics. As an example, the following reaction network is considered (Fig. 12.7) consisting of five essential species ($N^\star = 5$). The species B has three daughter species C_1, C_2, C_3. The reaction network of Fig. 12.7 can be decomposed into three serial reaction chains: $A \to B \to C_1$, $A \to B \to C_2$ and $A \to B \to C_3$. Accordingly, the following system of transport equations is considered:

Table 12.3 Problem parameters used for the 1D multispecies mass transport with serial-parallel reactions

Quantity	Symbol	Value	Unit
Extended length of column	$2L$	80	m
Longitudinal dispersivity	β_L	10	m
Pore velocity	v	0.4	$\mathrm{m\,d^{-1}}$
Molecular diffusion	D	0	$\mathrm{m^2\,s^{-1}}$
Dispersion	$\mathcal{D} = D + \beta_L v$	$4.63 \cdot 10^{-5}$	$\mathrm{m^2\,s^{-1}}$
Rate constant of species A	k_A	0.2	$\mathrm{d^{-1}}$
Rate constant of species B	k_B	0.1	$\mathrm{d^{-1}}$
Rate constant of species C_1	k_{C_1}	0.02	$\mathrm{d^{-1}}$
Rate constant of species C_2	k_{C_2}	0.02	$\mathrm{d^{-1}}$
Rate constant of species C_3	k_{C_3}	0.02	$\mathrm{d^{-1}}$
Stoichiometric coefficient of $A \rightarrow B$	ν_B	0.5	1
Stoichiometric coefficient of $B \rightarrow C_1$	ν_{C_1}	0.3	1
Stoichiometric coefficient of $B \rightarrow C_2$	ν_{C_2}	0.2	1
Stoichiometric coefficient of $B \rightarrow C_3$	ν_{C_3}	0.1	1
IC's and BC's			
Initial condition (IC) of C_k $(k = A, B, C_1, C_2, C_3)$	$C_{k,0}$	0	$\mathrm{mg\,l^{-1}}$
Dirichlet-type BC of species C_A at $x = 0$	C_{AD}	1	$\mathrm{mg\,l^{-1}}$
Dirichlet-type BC of species C_k at $x = 0$ $(k = B, C_1, C_2, C_3)$	C_{kD}	0	$\mathrm{mg\,l^{-1}}$
Natural BC for species C_k at $x = 2L$ $(k = A, B, C_1, C_2, C_3)$	$q_{n_{kC}} = -\mathcal{D}\nabla C_k \cdot \boldsymbol{n}$	0	$\mathrm{gm^{-2}\,d^{-1}}$
FEM			
Space increment	$\Delta x = 2L/600$	0.13333	m
Initial time step size	Δt_0	10^{-3}	d
RMS error tolerance (AB/TR)	ϵ	10^{-4}	1
Simulation time period	t_{end}	40	d

$$
\begin{aligned}
\frac{\partial C_A}{\partial t} - \mathcal{D}\frac{\partial^2 C_A}{\partial x^2} + v\frac{\partial C_A}{\partial x} &= -k_A\, C_A \\
\frac{\partial C_B}{\partial t} - \mathcal{D}\frac{\partial^2 C_B}{\partial x^2} + v\frac{\partial C_B}{\partial x} &= \nu_B\, k_A\, C_A - k_B\, C_B \\
\frac{\partial C_{C_1}}{\partial t} - \mathcal{D}\frac{\partial^2 C_{C_1}}{\partial x^2} + v\frac{\partial C_{C_1}}{\partial x} &= \nu_{C_1}\, k_B\, C_B - k_{C_1}\, C_{C_1} \\
\frac{\partial C_{C_2}}{\partial t} - \mathcal{D}\frac{\partial^2 C_{C_2}}{\partial x^2} + v\frac{\partial C_{C_2}}{\partial x} &= \nu_{C_2}\, k_B\, C_B - k_{C_2}\, C_{C_2} \\
\frac{\partial C_{C_3}}{\partial t} - \mathcal{D}\frac{\partial^2 C_{C_3}}{\partial x^2} + v\frac{\partial C_{C_3}}{\partial x} &= \nu_{C_3}\, k_B\, C_B - k_{C_3}\, C_{C_3}
\end{aligned}
\tag{12.61}
$$

The RHS's of (12.61) represent the reaction rates R_A, R_B, R_{C_1}, R_{C_2} and R_{C_3}. In (12.61) $\mathcal{D} = D + \beta_L\, v$ is a constant dispersion coefficient, x is the 1D coordinate, v is a constant pore velocity, k_k $(k = A, B, C_1, C_2, C_2)$ are 1st-order rate constants and ν_k are corresponding stoichiometric coefficients. All species are diluted chemicals in a mobile liquid phase. The transport parameters assumed for this problem are listed in Table 12.3. There is no need to specify the porosity ε.

To simulate the 5-species transport problem the column of its double extent $2L$ is uniformly discretized by 600 linear elements. The automatic AB/TR time stepping

procedure is applied. The simulation results can be compared to the analytical solution presented by Sun et al. [504]. Suppose the following IC's and BC's

$$\begin{array}{lll} C_k(x,0) = 0 & (k = A, B, C_1, C_2, C_2) & x \geq 0 \\ C_A(0,t) = 1 & & t > 0 \\ C_k(0,t) = 0 & (k = B, C_1, C_2, C_2) & t > 0 \\ C_k(\infty,t) = 0 & (k = A, B, C_1, C_2, C_2) & t > 0 \end{array} \tag{12.62}$$

the basic equation system (12.61) rewritten for the species k in the form

$$\mathcal{L}(C_k) = \nu_k \, k_{k-1} \, C_{k-1} - k_k \, C_k \tag{12.63}$$

where $\mathcal{L}(.)$ represents the differential operator, can be transformed by introducing the auxiliary variable a_k defined as

$$a_k = C_k + \begin{cases} 0 & k = 1 \\ \displaystyle\sum_{j=1}^{k-1} \prod_{i=j}^{k-1} \frac{\nu_{i+1} \, k_i}{k_i - k_k} C_j & k > 1 \end{cases} \tag{12.64}$$

to obtain the reactive transport equations in terms of a_k, viz.,

$$\mathcal{L}(a_k) = -k_k \, a_k \quad \forall k = 1, 2, \ldots, N^\star \tag{12.65}$$

Note that for $k = 1$ the transport equation (12.65) in terms of the first auxiliary variable is identical to the original equation (12.63) since $a_k = C_k$. The substituted equations (12.65) can be easily solved by the basic analytical formula

$$a_k(x,t) = \frac{a_{k0}}{2} \exp\left(\frac{vx}{2\mathcal{D}}\right) \left[\exp(-u_k x) \operatorname{erfc}\left(\frac{x - t\sqrt{v^2 + 4k_k\mathcal{D}}}{2\sqrt{\mathcal{D}t}} \right) + \exp(u_k x) \operatorname{erfc}\left(\frac{x + t\sqrt{v^2 + 4k_k\mathcal{D}}}{2\sqrt{\mathcal{D}t}} \right) \right] \tag{12.66}$$

where

$$u_k = \sqrt{\frac{v^2}{4\mathcal{D}^2} + \frac{k_k}{\mathcal{D}}} \tag{12.67}$$

and a_{k0} is the IC in terms of the auxiliary variable. The solutions of all concentrations C_k in the real untransformed domain can be determined by a successive substitution process using (12.64) in a reverse way

Table 12.4 Species ID's used in Sun et al.'s 1D problem

ID (= k)	Phase	Name
1	Liquid	A
2	Liquid	B
3	Liquid	C_1
4	Liquid	C_2
5	Liquid	C_3

$$C_k = a_k - \begin{cases} 0 & k = 1 \\ \sum_{j=1}^{k-1} \prod_{i=j}^{k-1} \frac{\nu_{i+1} k_i}{k_i - k_k} C_j & k > 1 \end{cases} \tag{12.68}$$

where a_k is the solution from (12.66). Note that for evaluating the analytical exp(.)erfc(.) expressions in (12.66) the more suitable exf(., .) function is applied as already introduced in Sect. 12.5.1.

The infinite BC in (12.62) used in the analytical solution cannot be applied in the numerical context and is replaced by a natural Neumann-type BC imposed at the outlet boundary section of the double length $2L$ of the column, cf. Table 12.3. The reaction kinetics for the present problem is of a *degradation type*. We employ FEFLOW's reaction kinetics editor (see Sect. 5.5.4) to specify the reaction rates R_k as follows:

$$\begin{aligned} R_1 &= -\text{Rate}_1 \cdot C_1 \\ R_2 &= 0.5 \cdot \text{Rate}_1 \cdot C_1 - \text{Rate}_2 \cdot C_2 \\ R_3 &= 0.3 \cdot \text{Rate}_2 \cdot C_2 - \text{Rate}_3 \cdot C_3 \\ R_4 &= 0.2 \cdot \text{Rate}_2 \cdot C_2 - \text{Rate}_4 \cdot C_4 \\ R_5 &= 0.1 \cdot \text{Rate}_2 \cdot C_2 - \text{Rate}_5 \cdot C_5 \end{aligned} \tag{12.69}$$

In (12.69) the parameters Rate_k represent the reaction constants k_k of Table 12.3. The used species ID's are linked to the species names and phases as summarized in Table 12.4. A comparison of the computational results with the analytical solutions gives perfect agreements as exhibited in Fig. 12.8. The simulation by using the parameters and conditions as listed in Table 12.3 takes 72 time steps of variable length.

12.5.3.2 Sun et al.'s 3D First-Order Degradation Reaction Kinetics Problem

Sun et al. [503] have extended their analytical approach to 3D problems for homogeneous parameters and steady-state flow regimes. The solutions are demonstrated for a four-species transport in a 3D aquifer of $L \times D \times B = 100\,\text{m} \times 41\,\text{m} \times 25\,\text{m}$. For the finite-element analysis the symmetric half-domain is discretized by $120 \times 37 \times 50 = 222{,}000$ linear brick (hexahedral) elements consisting of 234,498 nodes as shown in Fig. 12.9.

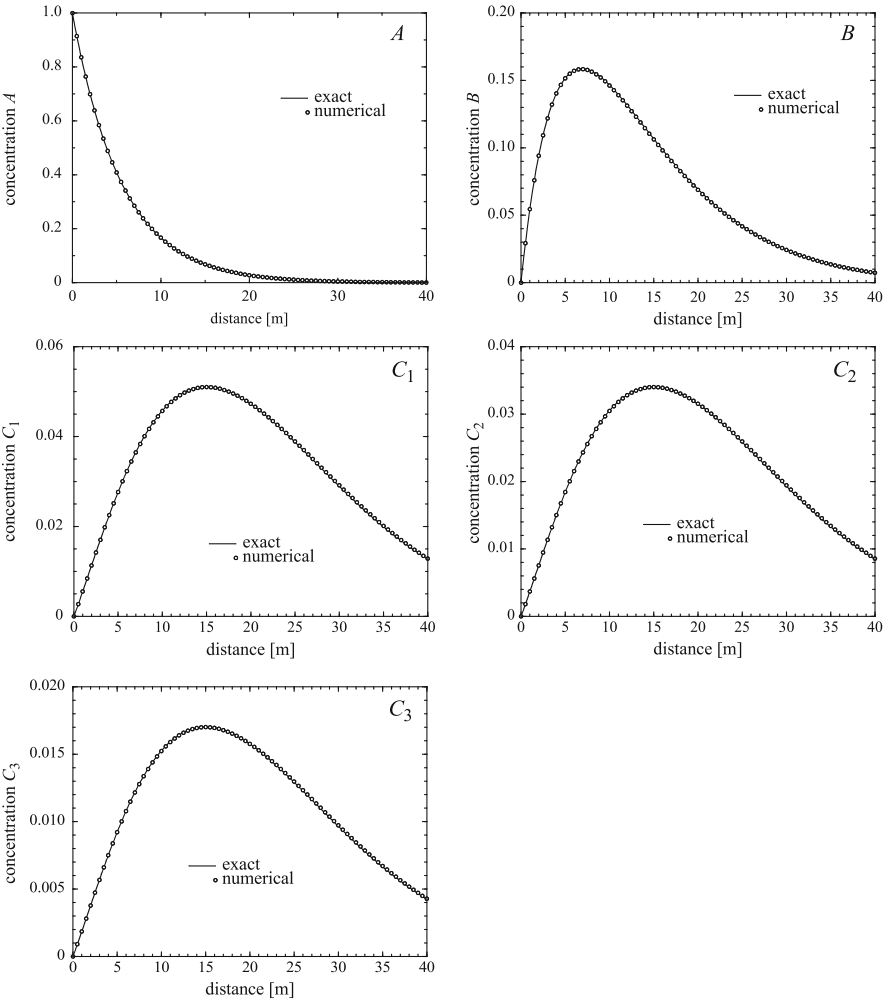

Fig. 12.8 Concentration profiles for the five species across the column of length L after $t = 40$ days of serial-parallel reactive transport: comparison of Sun et al.'s exact (analytical) solution to FEFLOW's numerical results

First-order reaction rates for the sequential reaction kinetics $C_1 \rightarrow C_2 \rightarrow C_3 \rightarrow C_4$ are given as follows

$$\begin{aligned} R_1 &= -k_1\, C_1 \\ R_2 &= k_1\, C_1 - k_2\, C_2 \\ R_3 &= k_2\, C_2 - k_3\, C_3 \\ R_4 &= k_3\, C_3 - k_4\, C_4 \end{aligned} \tag{12.70}$$

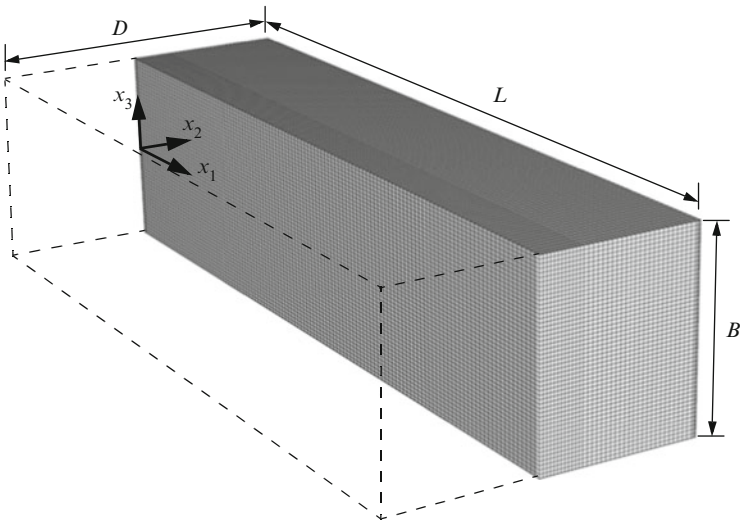

Fig. 12.9 Discretized 3D aquifer for Sun et al.'s problem. Structured mesh consists of 120×37×50 brick elements for the symmetric half-domain $L \times \frac{D}{2} \times B$

where k_k $(k = 1, 2, 3, 4)$ are rate constants, which are listed together with the remaining parameters in Table 12.5. All species are considered mobile in the liquid phase; porosity ε does not play a role. Unspecified BC's represent boundaries, at which natural BC's are imposed.

The obtained results are shown in Figs. 12.10 and 12.11. The concentration contours reveal differences between the analytical and numerical solutions. In the finite-element analysis the aquifer is finite and natural Neumann-type BC's (zero concentration gradients) are applied at the outer border faces of the discretized 3D domain. Unlike, in the analytical solution the aquifer domain is considered semi-infinite. Furthermore, Sun et al. [503] used an alternative dispersion model, where different transverse dispersivities in the horizontal and vertical directions are applied. In the FEFLOW simulations the Bear-Scheidegger dispersion model (12.3) is preferred with only one transverse dispersion parameter (Table 12.5).

12.5.3.3 Rate-Limited Desorption and Decay: Comparison to Fry et al.'s Analytical Solution

Fry et al. [179] studied rate-limited desorption and 1st-order decay on the feasibility of in situ bioremediation of contaminated groundwater by using analytical solutions. The conceptual model is shown in Fig. 12.12. A remedial pump-and-treat scheme is considered assuming conditions of 1D, steady-state groundwater flow through a homogeneous and isotropic aquifer. The modeled portion of the aquifer is bounded by injection and extraction wells (see control volume drawn in Fig. 12.12).

Table 12.5 Problem parameters used for the 3D multispecies mass transport with 1st-order degradation reaction kinetics

Quantity	Symbol	Value	Unit
Domain measure (length; half-with; thickness)[a]	$L; \frac{D}{2}; B$	$100; \frac{41}{2}; 25$	m
Longitudinal dispersivity	β_L	1.5	m
Transverse dispersivity	β_T	0.3	m
Pore velocity	v	0.2	$\mathrm{m\,d^{-1}}$
Molecular diffusion ($k = 1, 2, 3, 4$)	D_k	0	$\mathrm{m^2\,s^{-1}}$
Rate constant of species C_1	k_1	0.05	$\mathrm{d^{-1}}$
Rate constant of species C_2	k_2	0.02	$\mathrm{d^{-1}}$
Rate constant of species C_3	k_3	0.01	$\mathrm{d^{-1}}$
Rate constant of species C_4	k_4	0.005	$\mathrm{d^{-1}}$
IC's and BC's			
Initial condition (IC) of C_k ($k = 1, 2, 3, 4$)	$C_{k,0}$	0	$\mathrm{mg\,l^{-1}}$
Dirichlet-type BC of species C_1 at ($x_1 = 0, 0 \le x_2 \le 5.5\,\mathrm{m}, -2.5\,\mathrm{m} \le x_3 \le 2.5\,\mathrm{m}$)	C_{1D}	1	$\mathrm{mg\,l^{-1}}$
Dirichlet-type BC of species C_1 at ($x_1 = 0, x_2 > 5.5\,\mathrm{m}, x_3 < -2.5\,\mathrm{m}, x_3 > 2.5\,\mathrm{m}$)	C_{1D}	0	$\mathrm{mg\,l^{-1}}$
Dirichlet-type BC of species C_k ($k = 2, 3, 4$) at ($x_1 = 0, 0 \le x_2 \le 20.5\,\mathrm{m}, -12.5\,\mathrm{m} \le x_3 \le 12.5\,\mathrm{m}$)	C_{kD}	0	$\mathrm{mg\,l^{-1}}$
FEM			
3D mesh of $120 \times 37 \times 50$ brick elements (Fig. 12.9), GFEM and AB/TR			
Initial time step size	Δt_0	10^{-7}	d
RMS error tolerance (AB/TR)	ϵ	10^{-4}	1
Simulation time period	t_{end}	400	d

[a] Measures and origin of coordinate system (x_1, x_2, x_3) defined in Fig. 12.9

The study concerns a method of restoration of a contaminated aquifer domain, where organic compounds are degraded by indigenous or introduced microorganisms. Degradation of the contaminant is represented by a 1st-order decay, where the rate of degradation is a function of the contaminant concentration in the aqueous (liquid) phase. Desorption is described using 1st-order kinetics, where the rate of mass transfer of contaminant from the solid phase to the aqueous phase depends on the concentration gradient between the two phases and a single rate coefficient. The following 1D two-species transport equations are considered (written in the present notation), which is a *one-site kinetic model* [351, 542] with linear kinetic sorption and decay in the aqueous phase:

$$\begin{aligned} \varepsilon \frac{\partial C}{\partial t} + \varepsilon_s \frac{\partial S}{\partial t} + q \frac{\partial C}{\partial x} - \mathcal{D} \frac{\partial^2 C}{\partial x^2} &= -\varepsilon \vartheta C \\ \varepsilon_s \frac{\partial S}{\partial t} &= \varepsilon_s \alpha (\rho^s K^d C - S) \end{aligned} \tag{12.71}$$

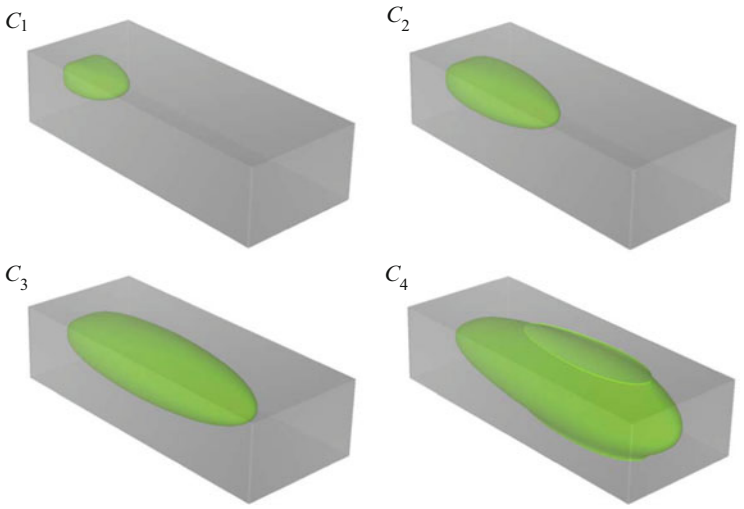

Fig. 12.10 FEFLOW results of the 3D 0.01 isosurface concentration for the four species C_1, C_2, C_3 and C_4 after $t = 400$ days

or

$$\begin{aligned} \varepsilon \frac{\partial C}{\partial t} + q \frac{\partial C}{\partial x} - \mathcal{D} \frac{\partial^2 C}{\partial x^2} &= R_C \\ \varepsilon_s \frac{\partial S}{\partial t} &= R_S \end{aligned} \tag{12.72}$$

with

$$\begin{aligned} R_C &= -(\varepsilon \vartheta + \varepsilon_s \rho^s \alpha K^d) C + \varepsilon_s \alpha S \\ R_S &= \varepsilon_s \alpha (\rho^s K^d C - S) \end{aligned} \tag{12.73}$$

where C is the aqueous concentration (at liquid phase), S is the sorbed concentration (at solid phase), $\mathcal{D} = \varepsilon D + \beta_L q$ is the hydrodynamic dispersion coefficient, $\varepsilon_s = 1 - \varepsilon$ is the solid volume fraction, ρ^s is the solid density, K^d is the distribution coefficient (cf. Table 3.8) and α is the 1st-order desorption rate constant.

The aquifer is initially contaminated and concentrations C and S are uniform throughout the control volume. Furthermore, the sorbed and aqueous phases are initially in linear equilibrium as described with the distribution coefficient K^d. These IC's are stated as

$$\begin{aligned} C(x,0) &= C_0 \qquad (0 \le x \le L) \\ S(x,0) &= S_0 \qquad (0 \le x \le L) \\ S_0 &= \rho^s K^d C_0 \end{aligned} \tag{12.74}$$

where C_0 is the aqueous concentration at $t = 0$, S_0 is the sorbed concentration at $t = 0$ and L is the length of the control volume (Fig. 12.12).

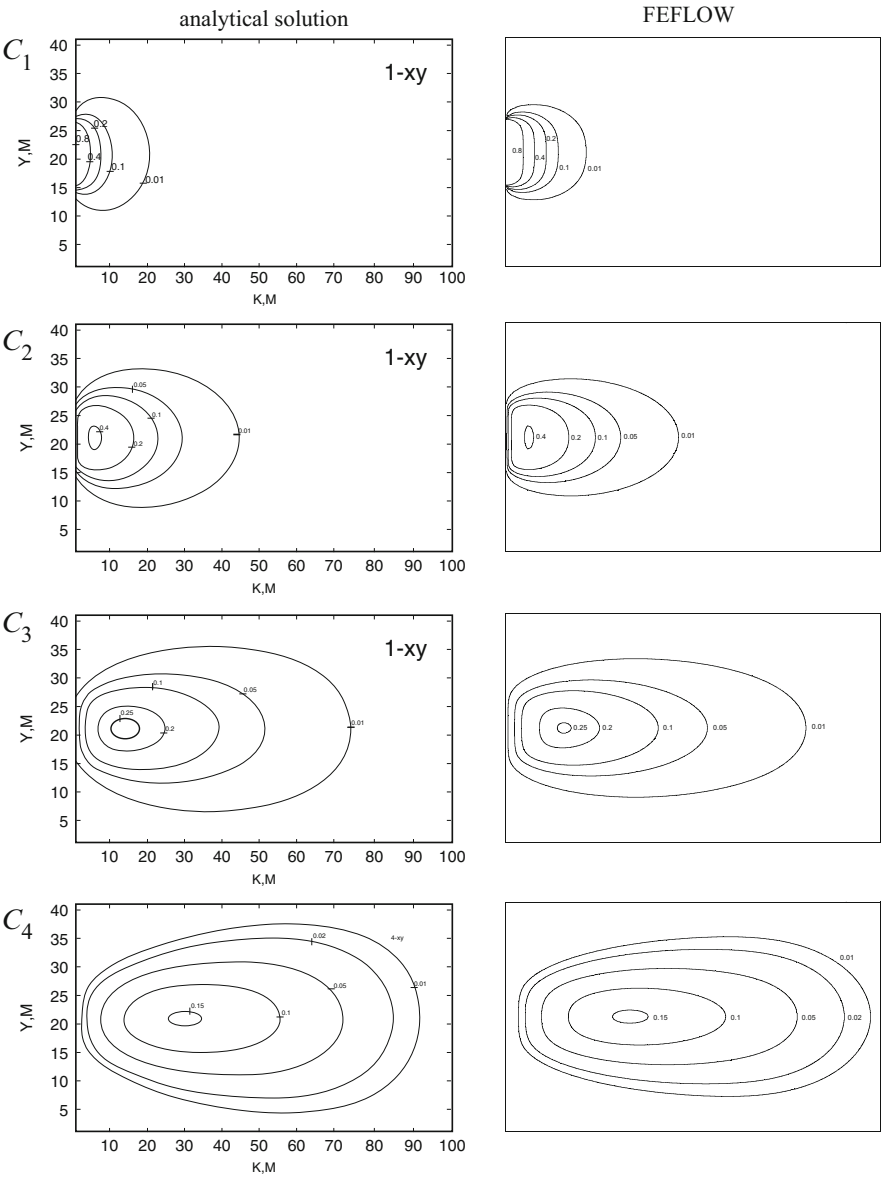

Fig. 12.11 Comparison of Sun et al.'s analytical solution [503] (*left*) with FEFLOW results (*right*): concentration contours of the four species C_1, C_2, C_3 and C_4 in the $x_1 - x_2$−plane at $x_3 = 13$ m and $t = 400$ days

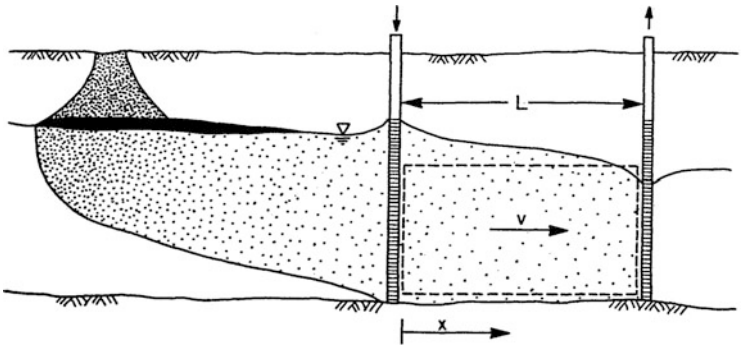

Fig. 12.12 Conceptual model of reacting contaminant transport in groundwater by Fry et al. [179]

At the control-volume inlet ($x = 0$) the contaminant flux due to advection and dispersion is zero at all times. At the control-volume exit ($x = L$) the concentrations are uniform with distance. Thus, the following BC's hold:

$$\begin{aligned} -\mathcal{D}\frac{\partial C}{\partial x}(0,t) + qC(0,t) = 0 \quad t > 0 \\ -\mathcal{D}\frac{\partial C}{\partial x}(L,t) = 0 \quad t > 0 \end{aligned} \tag{12.75}$$

A test case is considered for which the used parameters and conditions are listed in Table 12.6. Due to the BC's (12.75) the divergence form of the governing transport equations is used, which allows the input of the total (advective plus dispersive) mass flux at the boundary.

The reaction kinetics for the present problem is of a *degradation type*. We employ FEFLOW's reaction kinetics editor (see Sect. 5.5.4) to input the reaction rates (12.73), which are specified as follows (note that species ID 1 represents the aqueous species with concentration $C \equiv C_1$ and species ID 2 represents the sorbed species with concentration $S \equiv C_2$):

$$\begin{aligned} R_1 &= -(\text{Porosity}_1 \cdot \text{Rate}_1 + \text{Rate}_2 \cdot \text{Rb} \cdot \text{Kd}) \cdot C_1 + \text{Rate}_2 \cdot \text{SolidFrac}_2 \cdot C_2 \\ &\quad \text{Rb} = \text{SolidFrac}_2 \cdot 2.67 \quad \text{Kd} = 0.68 \\ R_2 &= \text{SolidFrac}_2 \cdot \text{Rate}_2 \cdot (\text{Rs} \cdot \text{Kd} \cdot C_1 - C_2) \\ &\quad \text{Rs} = 2.67 \quad \text{Kd} = 0.68 \end{aligned} \tag{12.76}$$

The parameters in (12.76) are related to the notation used in (12.73) as follows: $R_1 \equiv R_C$, $R_2 \equiv R_S$, $\text{Porosity}_1 \equiv \varepsilon$, $\text{Rate}_1 \equiv \vartheta$, $\text{Rate}_2 \equiv \alpha$, $\text{Rs} \equiv \rho^s$, $\text{Rb} \equiv \varepsilon_s \rho^s$, $\text{Kd} \equiv K^d$ and $\text{SolidFrac}_2 \equiv \varepsilon_s$. The species ID's are linked to the species names and phases as summarized in Table 12.7. The FEFLOW results for the problem are compared with the analytical solutions which are presented by Fry et al. [179].

Table 12.6 Parameters and conditions used for Fry et al.'s rate-limited desorption and decay transport problem in a column

Quantity	Symbol	Value	Unit
Column length	L	10	m
Constant flux	q	0.04	$\mathrm{m\,d^{-1}}$
Porosity	ε	0.4	1
Solid volume fraction	$\varepsilon_s = 1 - \varepsilon$	0.6	1
Distribution coefficient	K^d	0.68	$\mathrm{cm^3\,g^{-1}}$
Solid density	ρ^s	2.67	$\mathrm{g\,cm^{-3}}$
Decay rate	ϑ	0.1	$\mathrm{d^{-1}}$
Desorption rate constant	α	0.01	$\mathrm{d^{-1}}$
Molecular diffusion	D	0	$\mathrm{m^2\,s^{-1}}$
Longitudinal dispersivity	β_L	1	m
Dispersion	$\mathcal{D} = \varepsilon D + \beta_L q$	$4.63 \cdot 10^{-7}$	$\mathrm{m^2\,s^{-1}}$
IC's and BC's			
Initial condition (IC) of C	C_0	1	$\mathrm{mg\,l^{-1}}$
Initial condition (IC) of S	S_0	1.816	$\mathrm{mg\,l^{-1}}$
Natural BC of C at $x = 0$	$q_{n_C} = -\mathcal{D}\nabla C \cdot \boldsymbol{n} + qC\,\vert_{x=0}$	0	$\mathrm{gm^{-2}\,d^{-1}}$
Natural BC of C at $x = L$	$q_{n_C} = -\mathcal{D}\nabla C \cdot \boldsymbol{n}$	0	$\mathrm{gm^{-2}\,d^{-1}}$
FEM			
Uniform mesh consisting of 300 linear elements, GFEM			
Space increment	Δx	0.03333	m
Initial time step size[a]	Δt_0	10^{-5}	d
RMS error tolerance (AB/TR)	ϵ	10^{-4}	1
Simulation time period	t_{end}	10^3	d

[a] In addition, maximum rate of time step change $\Xi = \frac{\Delta t_{n+1}}{\Delta t_n} = 2$ and maximum time step size $\Delta t_{\max} = 0.5$ day

Table 12.7 Species ID's used in Fry et al.'s 1D problem

ID ($= k$)	Phase	Name
1	Liquid	C
2	Solid	S

As shown in Fig. 12.13 very good agreement with the analytical results is obtained. The FEFLOW simulation takes 2,039 time steps of variable length.

12.5.3.4 Two-Site Equilibrium/Kinetic Sorption with Degradation: Comparison to STANMOD Analytical Solutions

The two-site sorption concept presumes that sorption or exchange sites in soils can be classified into two fractions: one fraction (Type-1) on which sorption is assumed to be instantaneous, and another fraction (Type-2) on which sorption is considered to be time-dependent. The resulting two-site kinetic model interacts with a solid phase composed of such different constituents as soil minerals, organic matter and various

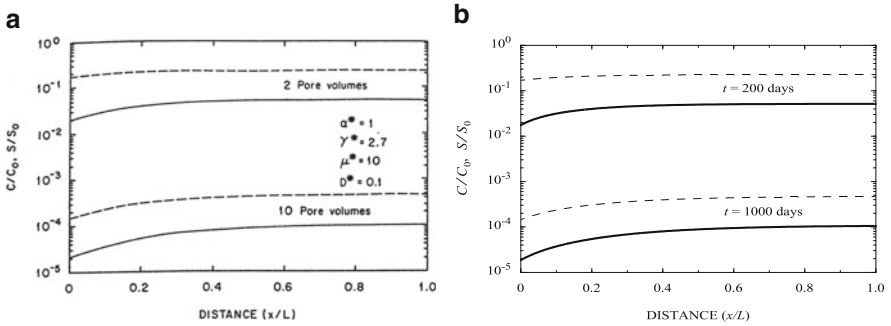

Fig. 12.13 Aqueous (C/C_0, *solid lines*) and sorbed (S/S_0, *dashed lines*) concentrations versus distance x at times $t = 200$ days and $t = 1{,}000$ days: (**a**) Fry et al.'s analytical solution [179] (pore volumes $= tq/(\varepsilon L)$) and (**b**) FEFLOW results

oxides. Studies in transport of pesticides indicate that the two-site kinetic model may well be suitable [542].

The derivation proceeds in the same fashion as for the one-site sorption model of the preceding Sect. 12.5.3.3. We introduce two different sorbed concentrations S_1 and S_2, where the first one is for Type-1 at equilibrium sites and the second one is for Type-2 at kinetic sites. Because Type-1 sites are always at equilibrium, sorption onto these sites is given by an adsorption function similar to (5.64), viz.,

$$S_1 = f\varphi\, C \tag{12.77}$$

where C is the aqueous concentration at liquid phase, f is the fraction of exchange sites assumed to be at equilibrium and φ is a sorption function. The kinetic part S_2 is subjected to a kinetic relationship in a form

$$S_2 \rightarrow (1-f)\varphi\, C \tag{12.78}$$

By using the equilibrium sorption (12.77) the Type-1 concentration S_1 can be eliminated (expressed by C) from the 3-species basic equations and only 2 species (namely C and S_2) have to be solved. Assuming a linear degradation for all species C, S_1 and S_2, as well as a Henry-type sorption for S_1, we found the following 2-species model equations for a *two-site kinetic sorption* [517,542] with degradation written in the present notation:

$$\begin{aligned} \varepsilon s \Re \frac{\partial C}{\partial t} + \boldsymbol{q}\cdot\nabla C - \nabla\cdot(\boldsymbol{D}\cdot\nabla C) &= R_C \\ \varepsilon_s \frac{\partial S_2}{\partial t} &= R_S \end{aligned} \tag{12.79}$$

with

$$\begin{aligned} R_C &= -\left[\alpha\varepsilon_s\tfrac{(1-f)}{f}\kappa + \varepsilon_s\kappa\vartheta_{S_1} + \varepsilon s\vartheta_C\right]C + \alpha\varepsilon_s S_2 \\ R_S &= \alpha\varepsilon_s\tfrac{(1-f)}{f}\kappa C - \varepsilon_s(\alpha + \vartheta_{S_2})S_2 \end{aligned} \tag{12.80}$$

and (cf. Table 3.8)

$$\begin{aligned} \Re &= 1 + \left(\tfrac{1-\varepsilon}{\varepsilon}\right)\kappa \\ \kappa &= f\rho^s K^d \end{aligned} \tag{12.81}$$

where C is the aqueous concentration (at liquid phase), S_1 is the Type-1 sorbed concentration (at solid phase), S_2 is the Type-2 sorbed concentration (at solid phase), $\varepsilon_s = 1-\varepsilon$ is the solid volume fraction, ρ^s is the solid density, K^d is the distribution coefficient (cf. Table 3.8), f is the fraction of exchange sites, α is the 1st-order kinetic rate coefficient, κ is the Henry adsorption coefficient (cf. Table 3.8), ϑ_{S_1} is the decay coefficient of sorbed species S_1, ϑ_{S_2} is the decay coefficient of sorbed species S_2 and ϑ_C is the decay coefficient of diluted species C. Note that the two-site adsorption model (12.80) reduces to the one-site fully kinetic adsorption model comparable to (12.73) if $f \to 0$, where the $(1-f)\kappa/f$ terms in (12.80) have to be replaced by $(1-f)\rho^s K^d$.

We solve the above two-site kinetic sorption equations for a 1D domain (column) of length L, for which analytical solutions are available [517,527,542]. To compare to analytical solutions the following dimensionless parameters are to be defined:

$$\beta = \frac{\Re}{\Re^\star}, \quad \Re^\star = 1 + \left(\frac{1-\varepsilon}{\varepsilon}\right)\frac{\kappa}{f}, \quad \omega = \alpha(1-\beta)\Re^\star\frac{L}{v}, \quad \mathrm{Pe} = \frac{qL}{\mathcal{D}} \tag{12.82}$$

where $q = \|\boldsymbol{q}\|$ is the constant 1D flux, $v = q/(s\varepsilon)$ is the constant 1D pore velocity and $\mathcal{D} = \|\boldsymbol{D}\|$ is the dispersion coefficient. With given parameters $\Re^\star$, β and ω, the model parameters κ, f and α can be specified as

$$\kappa = \frac{\varepsilon\beta(\Re^\star - 1) - (1-\beta)\varepsilon}{1-\varepsilon}, \quad f = \frac{\kappa(1-\varepsilon)}{(\Re^\star - 1)\varepsilon}, \quad \alpha = \frac{\omega}{(1-\beta)\Re^\star\frac{v}{L}} \tag{12.83}$$

Note that α is only defined if $\beta < 1$. Equations (12.79) with (12.80) are solved for an initially solute-free column subject to a pulse-type input BC. The IC's and BC's are stated as

$$\begin{aligned} C(x,0) &= 0 \quad (0 \le x \le L) \\ S_2(x,0) &= 0 \quad (0 \le x \le L) \end{aligned} \tag{12.84}$$

and

$$\begin{aligned} -\mathcal{D}\frac{\partial C}{\partial x}(0,t) + qC(0,t) &= \begin{cases} -qC_o & 0 < t \le t_o \\ 0 & t > t_o \end{cases} \\ -\mathcal{D}\frac{\partial C}{\partial x}(L,t) &= 0 \qquad t > 0 \end{aligned} \tag{12.85}$$

where C_o is the input concentration and t_o is the time duration of the applied solute pulse.

We consider the 1D column for a steady-state flow ($q = \text{const}$) and saturated conditions ($s = 1$). Furthermore, we assume that all decay coefficients are the same, i.e., $\vartheta = \vartheta_C = \vartheta_{S_1} = \vartheta_{S_2}$. Accordingly, a dimensionless decay parameter ξ is defined as

$$\xi = \frac{\vartheta L}{v} \tag{12.86}$$

The test case is considered for the dimensionless parameters with $\beta = 0.5$, $\Re^\star = 2.5$, $\omega = 0.5$, $\text{Pe} = 4.7$ and $\xi \in (0; 0.1; 0.3; 0.6; 1.0)$. In accordance with (12.83) the complete dataset used for the numerical simulation is listed in Table 12.8. Due to the BC's (12.85) the divergence form of the governing transport equations is used, which allows the input of the total (advective plus dispersive) mass flux at the boundary.

The reaction kinetics for the two-site kinetic transport problem is of a *degradation type*. We again prefer FEFLOW's reaction kinetics editor (see Sect. 5.5.4) to input the reaction rates (12.80), which are specified as follows (note that species ID 1 represents the aqueous species with concentration $C \equiv C_1$ and species ID 2 represents the sorbed species with concentration $S_2 \equiv C_2$):

$$\begin{aligned} R_1 &= -(\text{Rate}_2 \cdot \text{SolidFrac}_2 \cdot g \cdot K + \text{SolidFrac}_2 \cdot K \cdot \text{Rate}_1 + \\ &\quad \text{Porosity}_1 \cdot \text{Rate}_1) \cdot C_1 + \text{Rate}_2 \cdot \text{SolidFrac}_2 \cdot C_2 \\ &\quad f = 0.16667 \quad g = (1-f)/f \quad K = \text{Sorption}_1 \\ R_2 &= \text{Rate}_2 \cdot \text{SolidFrac}_2 \cdot g \cdot K \cdot C_1 - \text{SolidFrac}_2 \cdot (\text{Rate}_2 + \text{Rate}_1) \cdot C_2 \\ &\quad f = 0.16667 \quad g = (1-f)/f \quad K = \text{Sorption}_1 \end{aligned} \tag{12.87}$$

The parameters in (12.87) are related to the notation used in (12.80) as follows: $R_1 \equiv R_C$, $R_2 \equiv R_S$, $\text{Porosity}_1 \equiv \varepsilon$, $\text{Rate}_1 \equiv \vartheta$, $\text{Rate}_2 \equiv \alpha$, $\text{Sorption}_1 \equiv \kappa$ and $\text{SolidFrac}_2 \equiv \varepsilon_s$. The species ID's are linked to the species names and phases as summarized in Table 12.9.

The FEFLOW results for the problem are compared with the analytical solutions which are evaluated by using the STANMOD package [527]. We simulate the breakthrough characteristics for C and S_2 measured at the effluent boundary at $x = L$ for different decay parameters ξ (12.86). The plots are related to dimensionless aqueous and sorbed concentrations and , respectively, defined as

$$\hat{C} = \frac{C}{C_o}, \qquad \hat{S}_2 = \frac{S_2}{\left(\frac{1-f}{f}\right)\kappa C_o} \tag{12.88}$$

Figure 12.14 reveals a good agreement with the analytical solutions. The required number of adaptive AB/TR time steps is about 230.

Table 12.8 Parameters and conditions used for the two-site kinetic transport problem in a column

Quantity	Symbol	Value	Unit
Column length	L	10	m
Constant flux	q	0.04	$\mathrm{m\,d^{-1}}$
Porosity	ε	0.4	1
Pore velocity	$v = \frac{q}{\varepsilon}$	0.1	$\mathrm{m\,d^{-1}}$
Solid volume fraction	$\varepsilon_s = 1 - \varepsilon$	0.6	1
Henry coefficient	κ	0.16667	1
Fraction of exchange site	f	0.16667	1
Kinetic rate coefficient	α	0.004	$\mathrm{d^{-1}}$
Decay rate coefficient	ϑ	$\begin{cases} 0 \\ 0.001 \\ 0.003 \\ 0.006 \\ 0.01 \end{cases}$	$\mathrm{d^{-1}}$
Molecular diffusion	D	0	$\mathrm{m^2\,s^{-1}}$
Longitudinal dispersivity	β_L	2.128	m
Dispersion	$\mathcal{D} = \varepsilon D + \beta_L q$	$9.85 \cdot 10^{-7}$	$\mathrm{m^2\,s^{-1}}$
IC's and BC's			
Initial condition (IC) of C	C_0	0	$\mathrm{mg\,l^{-1}}$
Initial condition (IC) of S_2	S_0	0	$\mathrm{mg\,l^{-1}}$
Input concentration of C	C_o	1	$\mathrm{mg\,l^{-1}}$
Pulse duration	t_o	300	d
Neumann-type BC of C at $x = 0$	$q_{n_C} = -\mathcal{D}\nabla C \cdot \boldsymbol{n} + qC\|_{x=0}$	$\begin{cases} -qC_o & 0 < t \le t_o \\ 0 & t > t_o \end{cases}$	$\mathrm{gm^{-2}\,d^{-1}}$
Natural BC of C at $x = L$	$q_{n_C} = -\mathcal{D}\nabla C \cdot \boldsymbol{n}$	0	$\mathrm{gm^{-2}\,d^{-1}}$
FEM			
Uniform mesh consisting of 300 linear elements, GFEM			
Space increment	Δx	0.03333	m
Initial time step size	Δt_0	10^{-5}	d
RMS error tolerance (AB/TR)	ϵ	10^{-4}	1
Simulation time period	t_{end}	800	d

Table 12.9 Species ID's used for the two-site kinetic transport problem

ID ($= k$)	Phase	Name
1	Liquid	C
2	Solid	S_2

12.5.4 Multispecies Mass Transport of Sequential and Nonsequential Chlorinated Solvents Degradation Under Variable Aerobic-Anaerobic Conditions

In contrast to nonsequential (aerobic) degradation of chlorinated solvents, sequential dehalogenation is performed by anaerobic bacteria that cannot work under aerobic

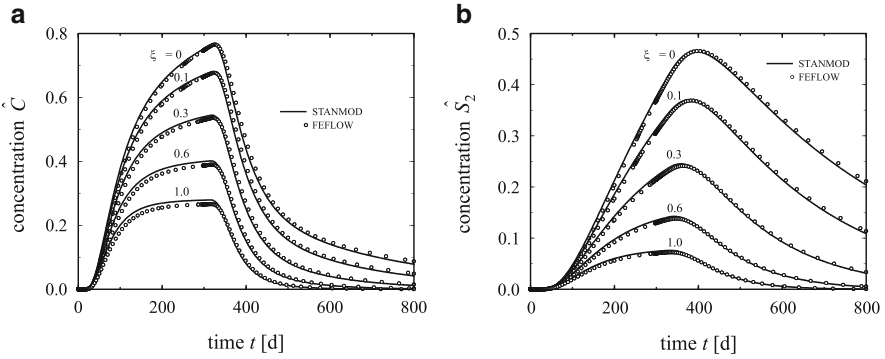

Fig. 12.14 FEFLOW results versus STANMOD solutions [527] for effluent breakthrough history at $x = L$ of (**a**) aqueous $\hat{C}$ and (**b**) sorbed $\hat{S}_2$ concentrations for different decay parameters ξ at Pe = 4.7, $\beta = 0.5$, $\omega = 0.5$, $\Re = 1.25$ and $t_o = 300$ days

conditions.[9] Both mechanisms can occur in the same contaminant plume depending on oxygen and nitrate concentrations. Monitoring the chloride released during the dehalogenation can be useful to locate the areas where dehalogenation occurs and to estimate degradation rates. This example simulation issues from a benchmark within the MACAOH (Modélisation, Atténuation, Charactérisation dans les Aquiféres des composés Organo-Halogénés) project [4] of the French Environment and Energy Management Agency (ADEME) with various university and private partners. The project focuses on chlorinated solvents, specifically PCE (perchloroethylene), TCE (trichloroethylene), DCE (cis- and trans-1,2-dichloroethylene) and VC (vinyl chloride). The aim of the benchmark was to evaluate the state of the art in the numerical simulation of the natural degradation of chlorinated solvents in aquifers in France.

A mixture of PCE and TCE is injected continuously in an initially uncontaminated 1D domain containing dissolved oxygen, nitrate and chloride. The initial aerobic conditions do not allow the degradation of PCE by anaerobic bacteria, but a slow complete mineralization of TCE is considered. Daughter products of TCE during the mineralization (H_2O and CO_2) are not simulated, except chloride ions. The oxygen concentration decreases as a consequence of the aerobic bacteria respiration. This behavior continues as long as the concentration of oxygen remains above a critical level. The reactions take place only in the liquid phase. Reaction and sorption with the solid phase are neglected.

Wiedemeier et al. [564] explained that anaerobic bacteria cannot work at oxygen concentrations greater than $0.5\,\mathrm{mg\,l^{-1}}$. When no more oxygen remains in water, aerobic bacteria use nitrate. After Wiedemeier et al. [564], anaerobic bacteria can

[9] FEFLOW results described in this section were obtained by D. Etcheverry† and Y. Rossier (France).

start the sequential reductive dechlorination of chlorinated solvents under nitrate concentrations smaller than $1\,\mathrm{mg\,l^{-1}}$.

In the MACAOH benchmark, it was assumed that the sequential degradation starts in the presence of nitrate as soon as the oxygen concentration reaches zero. Thus, once oxygen reaches sufficiently low concentration anywhere in the domain, the following reductive sequential degradation of chlorinated solvents starts

$$\mathrm{PCE} \overset{H^+,2e^-}{\longrightarrow} \mathrm{TCE} + \mathrm{Cl}^- \overset{H^+,2e^-}{\longrightarrow} \mathrm{DCE} + \mathrm{Cl}^- \overset{H^+,2e^-}{\longrightarrow} \mathrm{VC} + \mathrm{Cl}^- \tag{12.89}$$

The concentration of nitrate is supposed to decrease independently of other species, as soon as the oxygen concentration reaches zero, following a simple 1st-order degradation law.

The 1D equations of transport for the homogeneous reaction of nonretarded parent and daughter species can be written as

$$\begin{aligned}
\varepsilon\frac{\partial C_k}{\partial t} - \mathcal{D}\frac{\partial^2 C_k}{\partial x^2} + q\frac{\partial C_k}{\partial x} &= \varepsilon\left[\delta_k k_k^{\mathrm{anae}} C_k - (1-\delta_k) k_k^{\mathrm{ae}} C_k\right] \\
\varepsilon\frac{\partial C_j}{\partial t} - \mathcal{D}\frac{\partial^2 C_j}{\partial x^2} + q\frac{\partial C_j}{\partial x} &= \varepsilon\left[\delta_j k_j^{\mathrm{anae}} C_j - \delta_j \nu_{k,j} k_k^{\mathrm{anae}} C_k - (1-\delta_j) k_j^{\mathrm{ae}} C_j\right]
\end{aligned} \tag{12.90}$$

where k denotes the parent species (PCE to DCE), j the daughter product (TCE to VC), C_k and C_j the concentration of species k and j, respectively, k_k^{ae}, k_j^{ae}, k_k^{anae} and k_j^{anae} the 1st-order decay constants of species k and j under aerobic and anaerobic conditions, respectively, $\nu_{k,j}$ the stoichiometric coefficient for the degradation of species k to produce species j, δ_k and δ_j functions equal to 0 for degradation in aerobic conditions and equal to 1 for degradation in anaerobic conditions.

The reaction rates appearing on RHS's of (12.90) are described as follows:

Chlorinated solvents:

Under aerobic conditions, there is no sequential degradation and the reaction rates $R^{\mathrm{ae}}_{\mathrm{PCE,TCE,DCE,VC}}$ of chlorinated solvents in aerobic conditions simplify to

$$\begin{aligned}
R^{\mathrm{ae}}_{\mathrm{PCE}} &= 0 \\
R^{\mathrm{ae}}_{\mathrm{TCE}} &= -\varepsilon(k^{\mathrm{ae}}_{\mathrm{TCE}}\, C_{\mathrm{TCE}}) \\
R^{\mathrm{ae}}_{\mathrm{DCE}} &= -\varepsilon(k^{\mathrm{ae}}_{\mathrm{DCE}}\, C_{\mathrm{DCE}}) \\
R^{\mathrm{ae}}_{\mathrm{VC}} &= -\varepsilon(k^{\mathrm{ae}}_{\mathrm{VC}}\, C_{\mathrm{VC}})
\end{aligned} \tag{12.91}$$

Under anaerobic conditions, the sequential degradation from PCE to VC leads to reaction rates $R^{\mathrm{anae}}_{\mathrm{PCE,TCE,DCE,VC}}$ defined as follows

Table 12.10 1st-order decay rates and stoichiometric coefficients used for the MACAOH benchmark example

Species k	k_k^{anae} (d^{-1})	k_k^{ae} (d^{-1})	$\nu_{k,j}$ (1)
PCE	0.03	0	–
TCE	0.09	0.009	$\nu_{\text{PCE,TCE}} = 0.792$
DCE	0.009	0.15	$\nu_{\text{TCE,DCE}} = 0.738$
VC	0	0.24	$\nu_{\text{DCE,VC}} = 0.644$
O_2	0	0	–
$NO3^-$	0.1	0	–
Cl^-	0	0	–

$$\begin{aligned} R_{\text{PCE}}^{\text{anae}} &= -\varepsilon(k_{\text{PCE}}^{\text{anae}} C_{\text{PCE}}) \\ R_{\text{TCE}}^{\text{anae}} &= -\varepsilon(k_{\text{TCE}}^{\text{anae}} C_{\text{TCE}} - \nu_{\text{PCE,TCE}}\, k_{\text{PCE}}^{\text{anae}}\, C_{\text{PCE}}) \\ R_{\text{DCE}}^{\text{anae}} &= -\varepsilon(k_{\text{DCE}}^{\text{anae}} C_{\text{DCE}} - \nu_{\text{TCE,DCE}}\, k_{\text{TCE}}^{\text{anae}}\, C_{\text{TCE}}) \\ R_{\text{VC}}^{\text{anae}} &= -\varepsilon(k_{\text{VC}}^{\text{anae}} C_{\text{VC}} - \nu_{\text{DCE,VC}}\, k_{\text{DCE}}^{\text{anae}}\, C_{\text{DCE}}) \end{aligned} \tag{12.92}$$

Except for PCE that has no parent species, all reaction rates are made of an independent degradation term and of a production term dependent on the degradation of the parent species.

Oxygen:

Aerobic bacteria do not use oxygen in definite proportions during their respiration. The oxygen consumption was arbitrarily defined in the benchmark as follows

$$\frac{\partial C_{\text{O}_2}}{\partial t} = 4.5\frac{\partial C_{\text{TCE}}}{\partial t} + 4\frac{\partial C_{\text{DCE}}}{\partial t} + 3.5\frac{\partial C_{\text{VC}}}{\partial t} \tag{12.93}$$

From the conceptual model, the terms in DCE and VC are superfluous because they are not present in the system at the initial state and because TCE does not degrade into those compounds in aerobic conditions. Thus in this example simulation there cannot be DCE or VC under aerobic conditions and it follows from (12.93) that

$$R_{\text{O}_2}^{\text{ae}} = 4.5R_{\text{TCE}}^{\text{ae}} + 4R_{\text{DCE}}^{\text{ae}} + 3.5R_{\text{VC}}^{\text{ae}} \tag{12.94}$$

By definition there is no oxygen in anaerobic conditions, so that

$$R_{\text{O}_2}^{\text{anae}} = 0 \tag{12.95}$$

Chloride:

Chloride is released into the groundwater during the dehalogenation of chlorinated solvents. The relation

$$\frac{\partial C_{\text{Cl}^-}}{\partial t} = -1.068\frac{\partial C_{\text{TCE}}}{\partial t} - 0.712\frac{\partial C_{\text{DCE}}}{\partial t} - 0.552\frac{\partial C_{\text{VC}}}{\partial t} \tag{12.96}$$

Table 12.11 Parameters and conditions used for the MACAOH benchmark example

Quantity	Symbol	Value	Unit
Column length	L	250	m
Constant flux	q	0.4	$\mathrm{m\,d^{-1}}$
Porosity	ε	0.4	1
Pore velocity	$v = \frac{q}{\varepsilon}$	1	$\mathrm{m\,d^{-1}}$
Decay rates and stoichiometric coefficients of species: $k = \mathrm{PCE, TCE, DCE, VC, O_2, NO3^-, Cl^-}$ *are listed in Table 12.10*			
Longitudinal dispersivity	β_L	1	m
Retardation factor (no adsorption)	$\Re = \acute{\Re}$	1	1
Molecular diffusion	D	$1 \cdot 10^{-9}$	$\mathrm{m^2\,s^{-1}}$
Dispersion	$\mathcal{D} = \varepsilon D + \beta_L q$	$4.63 \cdot 10^{-6}$	$\mathrm{m^2\,s^{-1}}$
IC's and BC's			
Initial condition (IC) of C_{PCE}	$C_{\mathrm{PCE},0}$	0	$\mathrm{mg\,l^{-1}}$
Initial condition (IC) of C_{TCE}	$C_{\mathrm{TCE},0}$	0	$\mathrm{mg\,l^{-1}}$
Initial condition (IC) of C_{DCE}	$C_{\mathrm{DCE},0}$	0	$\mathrm{mg\,l^{-1}}$
Initial condition (IC) of C_{VC}	$C_{\mathrm{VC},0}$	0	$\mathrm{mg\,l^{-1}}$
Initial condition (IC) of $C_{\mathrm{O_2}}$	$C_{\mathrm{O_2},0}$	10	$\mathrm{mg\,l^{-1}}$
Initial condition (IC) of $C_{\mathrm{NO3^-}}$	$C_{\mathrm{NO3^-},0}$	20	$\mathrm{mg\,l^{-1}}$
Initial condition (IC) of $C_{\mathrm{Cl^-}}$	$C_{\mathrm{Cl^-},0}$	15	$\mathrm{mg\,l^{-1}}$
Dirichlet-type BC of species C_{PCE} at $x = 0$	$C_{\mathrm{PCE}\,D}$	3	$\mathrm{mg\,l^{-1}}$
Dirichlet-type BC of species C_{TCE} at $x = 0$	$C_{\mathrm{TCE}\,D}$	5	$\mathrm{mg\,l^{-1}}$
Dirichlet-type BC of species C_{DCE} at $x = 0$	$C_{\mathrm{DCE}\,D}$	0	$\mathrm{mg\,l^{-1}}$
Dirichlet-type BC of species C_{VC} at $x = 0$	$C_{\mathrm{VC}\,D}$	0	$\mathrm{mg\,l^{-1}}$
Dirichlet-type BC of species $C_{\mathrm{O_2}}$ at $x = 0$	$C_{\mathrm{O_2}\,D}$	10	$\mathrm{mg\,l^{-1}}$
Dirichlet-type BC of species $C_{\mathrm{NO3^-}}$ at $x = 0$	$C_{\mathrm{NO3^-}\,D}$	20	$\mathrm{mg\,l^{-1}}$
Dirichlet-type BC of species $C_{\mathrm{Cl^-}}$ at $x = 0$	$C_{\mathrm{Cl^-}\,D}$	15	$\mathrm{mg\,l^{-1}}$
Natural BC of all species k at $x = L$	$q_{n_k C} = -\mathcal{D}\nabla C_k \cdot \boldsymbol{n}$	0	$\mathrm{gm^{-2}\,d^{-1}}$
FEM			
Uniform mesh consisting of 250 linear elements, GFEM			
Space increment	Δx	1	m
Initial time step size[a]	Δt_0	10^{-3}	d
Maximum error tolerance (FE/BE)	ϵ	10^{-4}	1
Simulation time period	t_{end}	365	d

[a] In addition, maximum rate of time step change $\Xi = \frac{\Delta t_{n+1}}{\Delta t_n} = 1.1$ and maximum time step size $\Delta t_{\max} = 0.5$ day

Table 12.12 Reaction rates as defined in FEFLOW's reaction kinetics editor (cf. Sect. 5.5.4)

Reaction rate R_k (k = PCE, TCE, DCE, VC, O_2, $NO3^-$, Cl^-)			Comment
R_{PCE}	=	$\begin{cases} -\varepsilon(k^{\mathrm{anae}}_{\mathrm{PCE}} C_{\mathrm{PCE}}) & \text{if } C_{O_2} < 0.1 \\ 0 & \text{otherwise} \end{cases}$	$k^{\mathrm{ae}}_{\mathrm{PCE}} = 0$
R_{TCE}	=	$\begin{cases} -\varepsilon(k^{\mathrm{anae}}_{\mathrm{TCE}} C_{\mathrm{TCE}} - \nu_{\mathrm{PCE,TCE}} k^{\mathrm{anae}}_{\mathrm{PCE}} C_{\mathrm{PCE}}) & \text{if } C_{O_2} < 0.1 \\ -\varepsilon(k^{\mathrm{ae}}_{\mathrm{TCE}} C_{\mathrm{TCE}}) & \text{otherwise} \end{cases}$	
R_{DCE}	=	$\begin{cases} -\varepsilon(k^{\mathrm{anae}}_{\mathrm{DCE}} C_{\mathrm{DCE}} - \nu_{\mathrm{TCE,DCE}} k^{\mathrm{anae}}_{\mathrm{TCE}} C_{\mathrm{TCE}}) & \text{if } C_{O_2} < 0.1 \\ -\varepsilon(k^{\mathrm{ae}}_{\mathrm{DCE}} C_{\mathrm{DCE}}) & \text{otherwise} \end{cases}$	Degradation is supposed under aerobic conditions
R_{VC}	=	$\begin{cases} -\varepsilon(0 - \nu_{\mathrm{DCE,VC}} k^{\mathrm{anae}}_{\mathrm{DCE}} C_{\mathrm{DCE}}) & \text{if } C_{O_2} < 0.1 \\ -\varepsilon(k^{\mathrm{ae}}_{\mathrm{VC}} C_{\mathrm{VC}}) & \text{otherwise} \end{cases}$	No VC decay in anaerobic conditions ($k^{\mathrm{anae}}_{\mathrm{VC}} = 0$) but decay supposed under aerobic conditions
R_{O_2}	=	$\begin{cases} -\varepsilon(4.5 k^{\mathrm{ae}}_{\mathrm{TCE}} C_{\mathrm{TCE}} + 4 k^{\mathrm{ae}}_{\mathrm{DCE}} C_{\mathrm{DCE}} + 3.5 k^{\mathrm{ae}}_{\mathrm{VC}} C_{\mathrm{VC}}) & \text{if } C_{O_2} > 0.05 \\ 0 & \text{otherwise} \end{cases}$	
R_{NO3^-}	=	$\begin{cases} -\varepsilon(k^{\mathrm{anae}}_{NO3^-} C_{NO3^-}) & \text{if } C_{O_2} < 0.1 \\ 0 & \text{otherwise} \end{cases}$	Decay of nitrate starts under anaerobic conditions
R_{Cl^-}	=	$\begin{cases} \varepsilon(0.208 k^{\mathrm{anae}}_{\mathrm{PCE}} C_{\mathrm{PCE}} + 0.262 k^{\mathrm{anae}}_{\mathrm{TCE}} C_{\mathrm{TCE}} + 0.356 k^{\mathrm{anae}}_{\mathrm{DCE}} C_{\mathrm{DCE}} + 0.552 k^{\mathrm{anae}}_{\mathrm{VC}} C_{\mathrm{VC}}) & \text{if } C_{O_2} < 0.1 \\ \varepsilon(1.068 k^{\mathrm{ae}}_{\mathrm{TCE}} C_{\mathrm{TCE}} + 0.712 k^{\mathrm{ae}}_{\mathrm{DCE}} C_{\mathrm{DCE}} + 0.552 k^{\mathrm{ae}}_{\mathrm{VC}} C_{\mathrm{VC}}) & \text{otherwise} \end{cases}$	

is assumed under aerobic conditions, i.e., in terms of reaction rates

$$R^{\mathrm{ae}}_{Cl^-} = -1.068 R^{\mathrm{ae}}_{\mathrm{TCE}} - 0.712 R^{\mathrm{ae}}_{\mathrm{DCE}} - 0.552 R^{\mathrm{ae}}_{\mathrm{VC}} \tag{12.97}$$

For reductive dechlorination, different dechlorination kinetics is assumed, viz.,

$$\frac{\partial C_{Cl^-}}{\partial t} = -0.208 \frac{\partial C_{\mathrm{PCE}}}{\partial t} - 0.262 \frac{\partial C_{\mathrm{TCE}}}{\partial t} - 0.356 \frac{\partial C_{\mathrm{DCE}}}{\partial t} - 0.552 \frac{\partial C_{\mathrm{VC}}}{\partial t} \tag{12.98}$$

and

$$R^{\mathrm{anae}}_{Cl^-} = -0.208 R^{\mathrm{anae}}_{\mathrm{PCE}} - 0.262 R^{\mathrm{anae}}_{\mathrm{TCE}} - 0.356 R^{\mathrm{anae}}_{\mathrm{DCE}} - 0.552 R^{\mathrm{anae}}_{\mathrm{VC}} \tag{12.99}$$

Nitrate:

Nitrate is supposed to degrade at a given independent rate if the oxygen concentration is zero, which leads to the following reaction rates

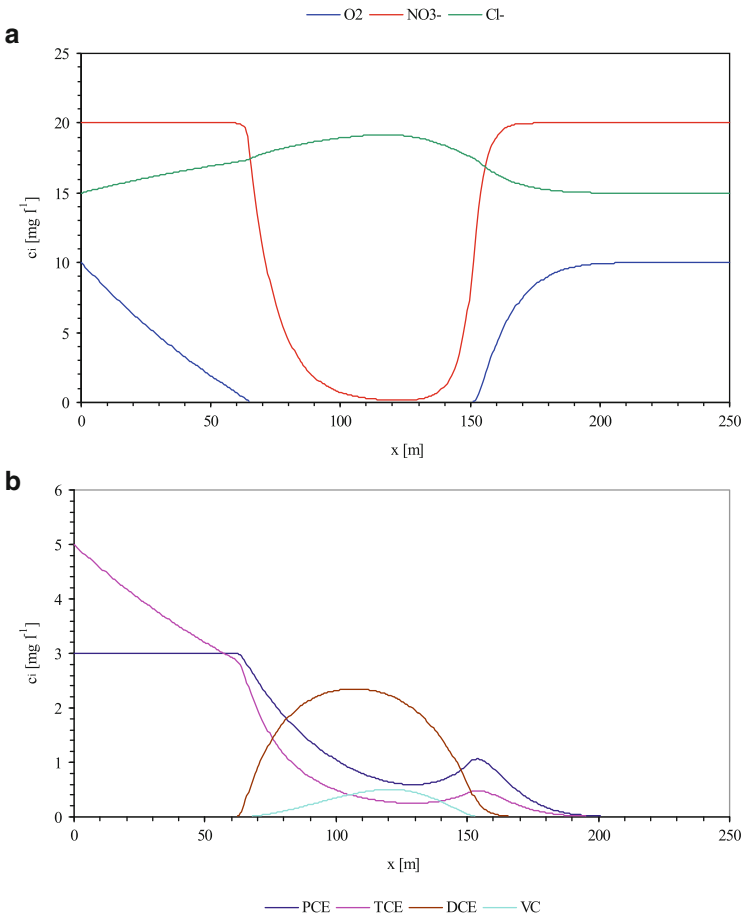

Fig. 12.15 Computed concentration profiles along the $x-$axis at 150 days for (**a**) oxygen, nitrate, chloride and (**b**) chlorinated solvents

$$\begin{aligned} R^{\text{ae}}_{\text{NO3}^-} &= 0 \\ R^{\text{anae}}_{\text{NO3}^-} &= -\varepsilon(k^{\text{anae}}_{\text{NO3}^-}\, C_{\text{NO3}^-}) \end{aligned} \tag{12.100}$$

1D steady flow and transient transport are supposed. The seven species simulated are PCE, TCE, DCE, VC, oxygen, nitrate and chloride. The aquifer length is 250 m, a constant Darcy flux q of 0.4 m d^{-1} is considered. For all species, porosity ε is 0.4, longitudinal dispersivity β_L is 1 m and retardation factor $\Re$ is 1. Steady Dirichlet-type species BC's of 3 mg l^{-1} for PCE, 5 mg l^{-1} for TCE, 0 mg l^{-1} for DCE and VC, 10 mg l^{-1} for oxygen, 20 mg l^{-1} for nitrate and 15 mg l^{-1} for chloride are applied at $x = 0$. IC's are assumed uniform, corresponding to the BC for oxygen, nitrate and chloride, and to zero for all chlorinated solvents. The 1st-order decay rates and

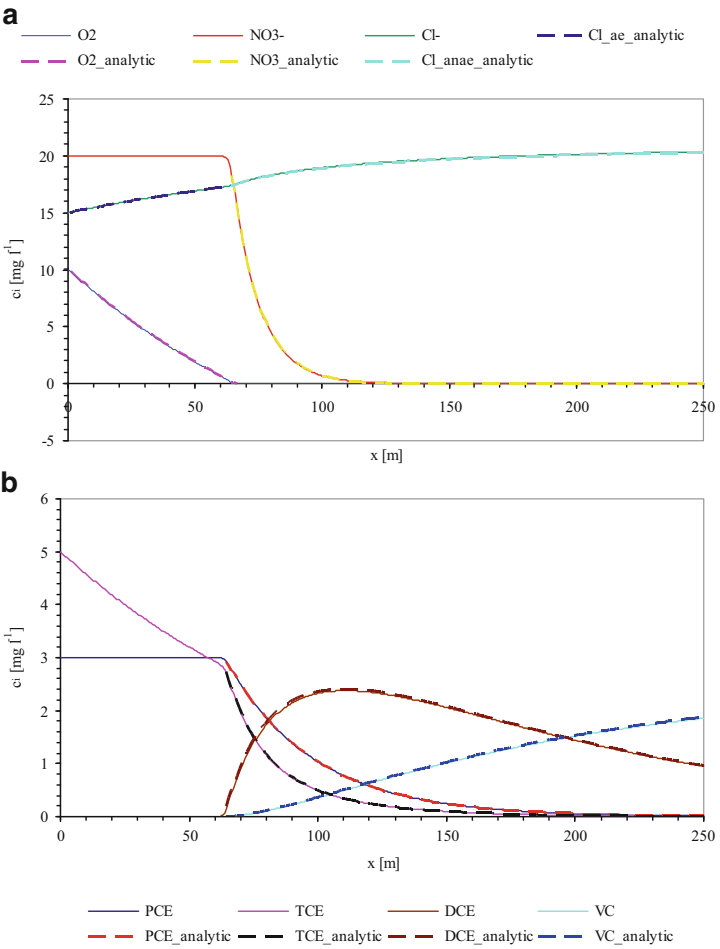

Fig. 12.16 Simulated versus analytical concentration profiles along the $x-$axis at steady state (365 days) for (**a**) oxygen, nitrate, chloride and (**b**) PCE, TCE, DCE, and VC. *Dashed lines* represent analytical solutions

stoichiometric coefficients are given in Table 12.10. Table 12.11 summarizes the simulation parameters and used conditions.

FEFLOW's versatile reaction kinetics editor (see Sect. 5.5.4) allows to easily define complex reaction rates. Particularly useful is the '*if otherwise*' construct to switch between aerobic and anaerobic behavior controlled via an oxygen concentration limit bounding the oxygen consumption below. It allows the combination of aerobic and anaerobic reaction rates in one composite reaction rate R_k for each species k. The reaction rates are entered in FEFLOW's reaction kinetics editor as listed in Table 12.12.

The simulation results are shown in Figs. 12.15 and 12.16 displaying the extent of the aerobic zone versus the anaerobic zone. At 150 days steady state is reached from $x = 0$ to $x = 65\,\text{m}$ for all species. Two separate aerobic zones appear from $x = 0$ to $65\,\text{m}$ and from $x = 165\,\text{m}$ to the outlet. Anaerobic conditions are found between these two zones allowing the degradation of nitrate and the sequential degradation of PCE into TCE, DCE and VC. Under aerobic conditions the fast increase in chloride is a result of the complete mineralization kinetics of TCE. After 365 days the anaerobic zone extends from $x = 65\,\text{m}$ to the outlet. The sequential degradation of chlorinated solvents leads to an accumulation of VC. The analytical solutions are obtained for each species, for the aerobic domain first, then for the anaerobic domain, by applying the decoupling solution of Sun et al. [503] (cf. Sect. 12.5.3). No method was found to solve the problem analytically in transient state because the solution must include a switching term between aerobic and anaerobic rates of reactions as a function of the oxygen concentrations, which are varying in space and in time. On the other hand, steady state offers by definition a stable space and time limit between aerobic and anaerobic conditions. Thus, it is possible to solve first the aerobic domain, and to take the concentrations calculated at the end of the domain as BC's for the calculations in the anaerobic domain. To avoid the development of a solution for parallel reactions, the contributions of each chlorinated solvent to the production of chloride under anaerobic conditions are solved separately and added to the chloride concentration obtained at steady state at the end of the aerobic zone. As revealed in Fig. 12.16 the numerical results for all species are quasi identical to the analytical solutions.